Hindawi
Advances in Civil Engineering
Volume 2022, Article ID 9512286, 26 pages
https://doi.org/10.1155/2022/9512286

Research Article

Nonlinear Behavior of Reinforced Concrete Frames Equipped with and without Steel Plate Shear Wall under Sequence of Real and Artificial Earthquakes

Hamze Rouhi and Majid Gholhaki

Department of Civil Engineering, Semnan University, Semnan, Iran

Correspondence should be addressed to Hamze Rouhi; hamzerohi@yahoo.com

Received 19 December 2021; Revised 24 July 2022; Accepted 4 November 2022; Published 23 November 2022

Academic Editor: Zhigang Zhang

There is a possibility of increasing structural damage in the sequential earthquake compared to the main earthquake according to past earthquakes. This study investigates the effects of seismic sequence on the behavior and increased response of reinforced concrete frames (RCF) with/without steel plate shear walls (SPSW). Four systems of 4, 8, 12, and 24 story, which represent low-, mid-, and high-rise structures, are designed and subjected to nonlinear time history analysis under critical single and consecutive records with real, repetitive, and randomized methods. The seismic scenarios used include sequential recorded critical earthquakes. The analysis showed that the predominant period of the after-shock significantly influences the post main-shock response. In RCF with and without SPSW, real seismic sequence increases the ratio of peak maximum interstory drift by an average of 2, 2 times the similar demand in the main shock, and increases the ratio of maximum ductility demand by 1.52 and 1.65 times in the structure, respectively. In an artificial sequence, the ratio of peak maximum interstory drift demand increase is in 100%, 150%, and 200% after-shocks, In the iteration method, it is equal to 1.2, 2.0, and 2.6 times the main shock in RCF with SPSW and 1.9, 3.2, and 4.8 times the main shock in RCF without SPSW. After-shocks may change the direction and magnitude of residual displacement in real and artificial seismic sequences. Continuation of the equation to calculate the demand for seismic sequence ductility was extracted.

1. Introduction

Because after-shocks usually occur shortly after the main-shock, and some of these after-shocks cause damage to the structure with a destructive force equal to that of the main-shock, strengthening the damaged structure of the main-shock in this short time interval is not possible, and to reduce the level of hazards, it is necessary to evaluate the performance of the damaged structure in general under the main-shock and after-shocks [1]. In 2011, about 100 after-shocks of magnitude six or more occurred four days after the Tohoku earthquake in Japan, causing structural damage and infrastructure damage [2]. In recent years, due to the increasing development of design methods and the tendency of codes to design based on performance, seismic assessment and performance of structures during earthquakes have become one of the most important issues in earthquake engineering. In the performance-based seismic design method, the structure is designed for different levels of expected performance, related to different levels of earthquake risk. An important step in performance-based design is to evaluate the nonlinear seismic response of structures. Accordingly, it is necessary to study the performance of structures during an earthquake and determine the capacity required to resist possible after-shocks in response to the structure and the possibility of the collapse of the building. The amount of damage to the structure is directly related to the demand for ductility [3]. Therefore, evaluating the relationship between these two parameters is very important. Current codes only evaluate the ductility demands of a

structure in the main-shock. Research in recent years has shown that the occurrence of after-shocks can significantly increase the demand for ductility of structures and lead to an increase in earthquake risk [4]. The main study of sequence earthquakes since the end of the nineteenth century has been done by Omori [5]. Omori concluded that the amount of deterioration during an after-shock was inversely related to the deterioration during the main-shock. One of the first studies by Mahin was conducted in 1980 [6]. Mahin realized that severe after-shocks could double the ductility and displacement demands of many elastoplastic one-degree-of-freedom systems. In addition to Mahin's work, there are several other studies to investigate the seismic performance of one-degree-of-free inelastic systems under a variety of ground motions in an earthquake sequence or various ground motions. Among these research works, we can mention the research work of Elnashai et al. in 1998 [7], Sunasaka and Kiremidjian in 2002 [8], Amadio et al in 2003 [9], Das et al. in 2007 [10], and Iancovivi and Georgiana in 2007 [11]. Hatzigeorgiou and Beskos in 2009 [12] proposed nonlinear displacement values suitable for sequence earthquakes, in addition to Hatzigeorgiou in 2010 [13] studied the demand for ductility and coefficient of the behavior of the nonlinear free degrees system under sequence earthquakes near and far-field. Hatzigeorgiou in 2010 [14] examined the response of one degree of freedom structures under sequence earthquakes near and far-field using artificial earthquakes and concluded that the use of the main-shock in evaluating the inelastic response of structures is contrary to certainty, and designers must pay attention to the effects of sequence earthquakes. Mustafa and Takewaki in 2011 [15] examined simple random models and showed the repetition of sequence earthquakes. In addition, they proposed the effects of sequence earthquakes on freedom multidegree systems. Hatzigeorgiou and Liolios in 2010 [16] investigated the effect of seismic sequence on the ductility demand of RCF. According to this research, the seismic sequence has an important effect on the response of the structure, and ductility demands in seismic sequence can be calculated with high accuracy using a combination of main-shock demands such as seismic sequence. Garcia and Negrete-Manriquez in 2011 [17] assessed the demand for drift in steel frames under sequence seismic records in the near and near-fields. The main purpose of this study was to investigate the relationship between the frequency content of the main-shock and after-shock, the effects of after-shocks on the drift, and residual drift of freedom multidegree systems and to evaluate the difference in response between real and artificial sequence earthquakes. Research by Efraimiadou et al. in 1997 [18], Di Sarno in 2013 [19], and Abdelnaby and Elnashai in 2014 [20] focused on multistory RCF. Almost all of this research has been done on the response of two-dimensional systems. Zhai et al. in 2012 [3] studied the response of inelastic main degree of freedom systems under a variety of ground motions. They compared the different responses of structural demand parameters in after-shocks, such as maximum acceleration, maximum velocity, maximum displacement, and residual displacement with their corresponding values in the main-shock and concluded that in potential after-shocks, there is an increase in the response of the structure, and after-shocks cannot always increase both components of maximum acceleration and maximum velocity in the structure in the same way. In other words, for a fixed structure, after-shocks may increase the maximum acceleration, while there is no maximum velocity. After-shock may also increase or decrease the residual displacement of structure due to the effects of the main-shock. Therefore, after-shocks can change the accumulation of damage to structures by affecting the displacement and sometimes reverse the results. Shin et al. in 2014 [21], by analysing the fragility of RCF, concluded the change in structural performance under sequence earthquake. Hatzivassiliou and Hatzigeorgiou in 2015 [4] investigated the effects of real seismic sequence with vertical earthquake components on regular and irregular three-dimensional concrete buildings. The most important result of this research is that the maximum story displacement of the structure under seismic sequence is more than main-shocks and the displacement and residual drift increase due to seismic sequence compared to the main-shock. Salimbahrami and Gholhaki in 2018 [22] conducted an analytical study to evaluate the effects of higher modes of RCF with thin SPSW under a simple pulse. According to their research, the demands of maximum displacement and force for different structures with the ratio of pulse period to the first mode period of vibration are equal to one, and with the increase of stories, the effects of higher modes decrease, and the most important effects of higher modes are roof shear force and base shear. In 2019, they also investigated the effect of higher modes and degrees of freedom on the coefficient of reduction of resistance in RCF with SPSW and the coefficient of reduction of earthquake resistance of far and near-field, which can be different, for a multidegree of freedom have corrected. Di Sarno and Pugliese in 2020 [23] assessed the seismic fragility of existing RC buildings with corroded bars under earthquake sequences. The outcomes of this numerical investigation showed that multiple excitations and corrosion significantly affect the seismic vulnerability of the investigated building; modified spectral acceleration intensity appeared to be the most effective intensity measure to assess the seismic fragility of corroded RC buildings. Di Sarno and Wu in 2021 [24] assessed the fragility of existing low-rise steel moment-resisting frames with masonry infills under main-shock-after-shock earthquake sequences. The assessment considered the effects of multiple earthquakes on the damage accumulation of steel frames. Comparative analyses were conducted among the main-shock-damaged structures considering three post-main-shock-damage levels, including no damage. The impact of after-shocks was then discussed for each main-shock-damage level in terms of the breakpoint that marks the onset of exceeding postmain-shock-damage level, as well as the probability of exceeding superior damage level due to more significant after-shocks. The evaluation of the efficiency of commonly used intensity measures of after-shocks was also carried out as part of the second phase of the assessment. Di Sarno and Pugliese in 2021 [25] studied the effects of main-shock-after-shock sequences on the fragility analysis of RC buildings with aging. The results of the comprehensive

numerical simulations contribute to providing relevant indications on the nonlinear response of existing corroded buildings under multiple excitations and highlight that current seismic codes are no longer conservative for such detrimental phenomena.

SPSW is a type of system suitable for earthquake, wind lateral loads consist of a series of separate panels, each panel is enclosed inside two beams and columns, and a steel plate is connected to the surrounding elements [26]. The use of SPSW due to stiffness, strength, and significant energy dissipation of seismic as an effective lateral system in seismic rehabilitation to increase the lateral strength and stiffness of buildings against earthquake (technical rehabilitation strategies) in steel structures is considered. Recently, due to the fact that the use of SPSW requires the use of environmental elements (beams and columns) with high rigidity, to increase the lateral strength and stiffness of concrete buildings with a moment-resisting frame, which naturally has such elements, has been used. Therefore, recently, the RCF with SPSW has been proposed as a new system against lateral loads [27].

Due to the novelty of this system, this system needs more numerical and laboratory studies. This research is also focused on to better understand this system. Numerous studies have been done on a type of structural system, including resisting moment frames, braced systems, and concrete shear walls under sequence earthquakes. However, the RCF with SPSW has been studied from various aspects recently, and therefore, the effect of sequence earthquakes (near and far-field) on this system has not been studied.

In this research, the effects of after-shocks on the response of the RCF with SPSW and residual displacement are studied. For this purpose, some sequence real and artificial records of far-filed and near-field, including the main-shock (MS) and after-shock (AS) records, have been used. Different scenarios include main-shock and after-shock in the far and near field has been used. In these scenarios, main-shock has been scaled to 0.3 g and different after-shock intensities of 0.15 g, 0.3 g, 0.45 g, and 0.6 g by back-to-back and randomized methods has been used. The ratio of peak maximum interstory and residual drift and critical scenario is detemined.

1.1. Research Method. The method used in this research is presented with a flowchart of Figure 1. As shown in this figure, to validate the numerical analysis process, a 3-story experimental model of a concrete frame equipped with a steel plate infill wall [28] whose specifications are presented in Figure 2 was simulated by making use of OpenSees software [29]. Four 2D frames including 4-, 8-, 12-, and 24-story equipped with steel shear walls were considered for the numerical analyses in this study. The 4-, 8-, 12-, and 24-story frames correspond to low, mid, and high-rise buildings, respectively. The first mode period of vibration of models (T_1) was extracted. The method for scaling earthquakes according to the standard of 2800 Iranian earthquakes is the same as in ASCE7-2010. The design spectrums of these codes are different for $T_1 > 1$ (s). With the first fundamental period greater than 1 second, the design spectrums of the standard of 2800 Iranian earthquake multiply coefficient equal 1.104 for the soil type III.

1.2. Numerical Modeling Validation. Validation of analytical models is one of the steps of research. To validate the model, the laboratory study of Choi and Park in 2011 [28] according to Figure 2(a) has been used. He conducted a laboratory study to investigate the cyclic behavior of walls consisting of boundary elements of RCF and thin steel sheets. To ensure the accuracy of the modeling, the numerical model of the laboratory sample was modeled and analysed in OpenSees finite element software [29]. For modeling, the nonlinear beam-column element has been used for the beam and column elements with deformation control, which can take into account the P-Δ effect and large deformations. The strip method has been used to model the steel plate [30]. In this method, a truss element is used to model the tensile strips. To model the wide plasticity of the elements in the program, the cross-sections of the beam and column elements are divided into some fibers. Concrete02 and reinforcing steel materials can model the downward part of the performance curves that have been used for modeling concrete and steel materials of reinforcements, respectively. To model the actual behavior of the strips that should not react when pressed, hysteretic materials are used, which with the three-line behavior in tension and pressure gives the strips the property that does not show resistance when under pressure and allows that the diagonal tensile field of a steel shear wall is well modeled. Also, the discussion of concrete confinement of columns is seen in the model. Numerical results from cyclic loading are compared with laboratory results (Figure 2(b)). The values of load-bearing capacity, initial stiffness, and energy absorption determined from the experiment and the corresponding simulated model are presented in Table 1. The comparison between the two diagrams in Figure 1(b) shows the acceptable accuracy in the modeling phase of this research. In the finite element modeling [29] and also in [28], any bond slip and fixed-end rotation are not considered.

To ensure that the perimeter columns can withstand the stresses due to the environmental loads along with the stresses due to the tensile field effect, it is necessary to check equation (5) for the plastic field of the columns:

$$M_{fpc} \geq \frac{\sigma_{ty} t h^2}{4} \cos^2 \alpha. \tag{5}$$

Equivalent tensile bracing [30] was used to model the SPSW in the design stages due to the impossibility of modeling the steel plate in the model geometry and its analysis by ETABS software. In the last two stories of the 24-story model, due to the negative shear in the braces, the use of an SPSW in these stories was avoided in the structure, and only the special RCF system was used to deal with the lateral force. Designed structural sections of 4, 8, 12, and 24-story models are presented in Tables 2–5.

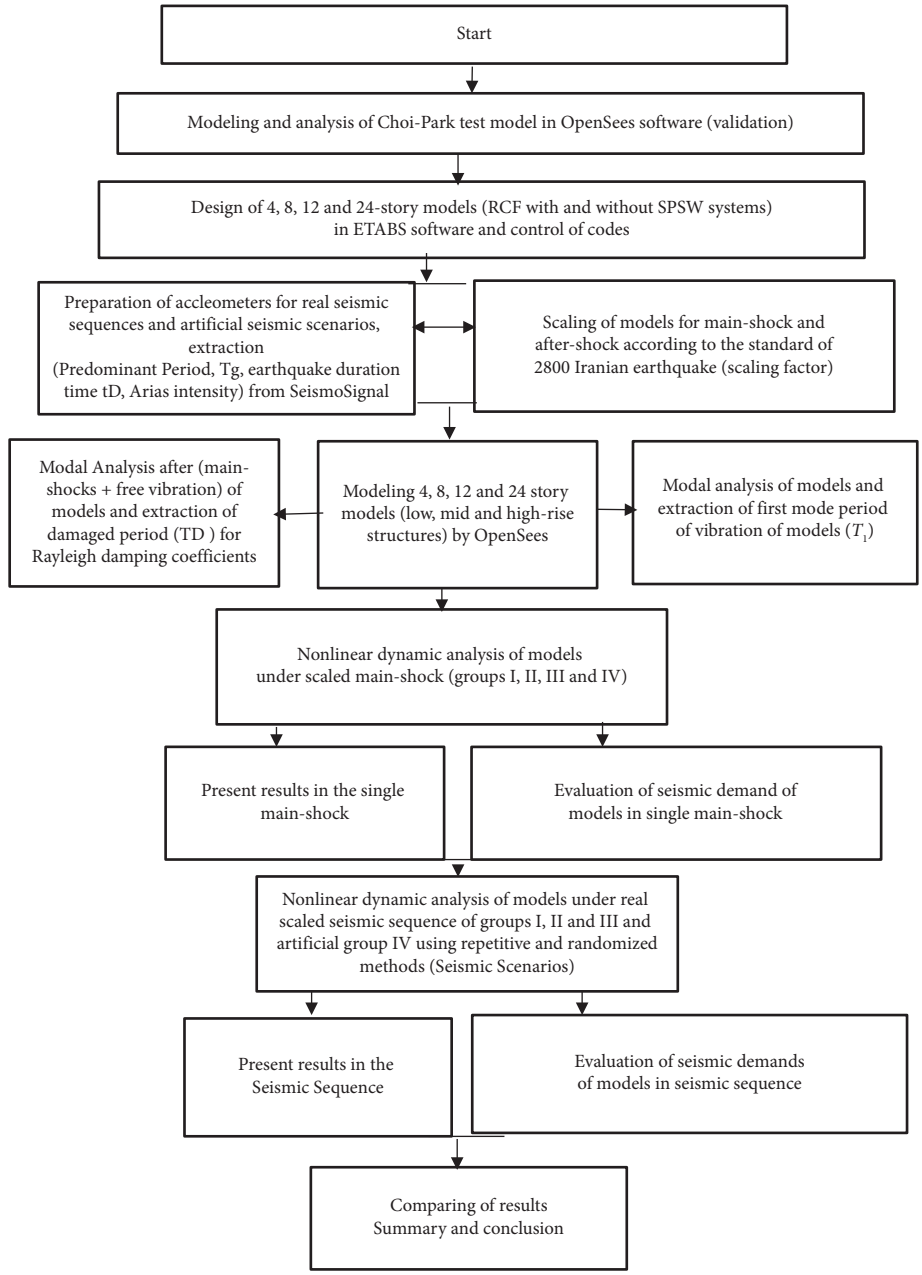

Figure 1: Flowchart of methodology.

2. Modeling of Case Study Structures

2.1. Modeling in ETABS Software and Design of SPSW. Regarding the classification of structural systems, some have considered the ratio of the height to the smallest horizontal dimension of the structure as a criterion for classifying buildings and height to the smallest dimension ratios greater than 1.5 π, between π and 1.5 π, between π and 0.5 π, and less than 0.5 π are known as super high, high, mid, and low-rise buildings, respectively [31]. Accordingly, in this research, four models of 4, 8, 12, and 24 story with height to the smallest dimension ratios of 0.54, 1.09, 1.63, and 3.26 in the classification of low, low, mid, and high-rise structures with a rectangular plan according to Figure 3(a), is selected with an RCF with SPSW and high ductility. The height of the stories of the models is 3.4 meters, and the roof is considered as a block joist. It is assumed that the building is located in a high seismic hazard zone resting on soil type III. The buildings are residential with moderate importance factor design. Concrete used in C25 grade concrete structures has a characteristic strength of 250 kg/cm^2 and rebar of type A3 with a yield stress of 4000 kg/cm^2. The steel used for equivalent braces is construction soft steel with a yield stress of 2400 kg/cm^2. In the analysis and design of the studied structures, the sixth [32] and ninth [33] national building regulations and the Iranian 2800 earthquake standard, and fourth edition [34] have been used; according to the sixth National Building Regulations, the deadweight load of stories and roof is 640 kg/m^2; the live

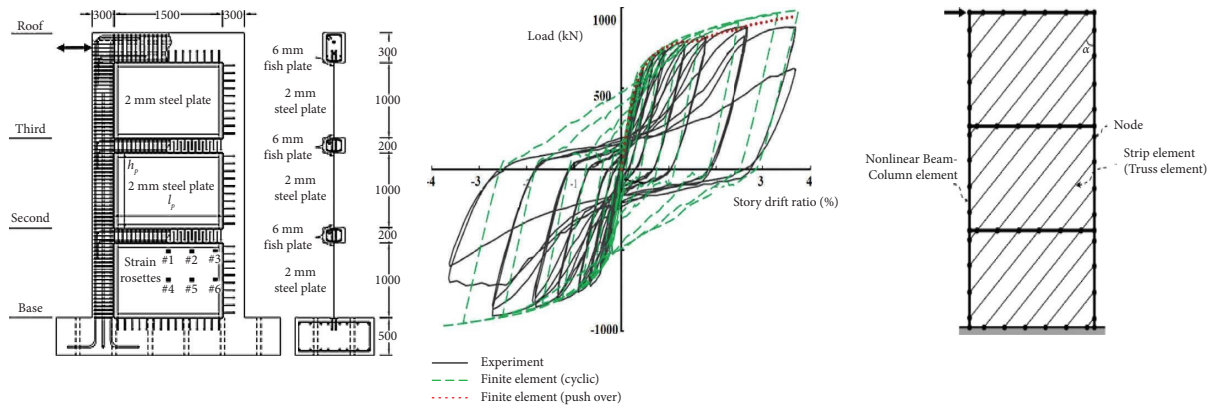

(a) (b) (c)

FIGURE 2: Numerical model validation. (a) Geometric and reinforcing details of the RCF with SPSW [28], (b) hysteresis curve of numerical model [29] and Choi and Park laboratory sample [28], (c) finite element model double-sided diagonal truss element in the cyclic analysis [28].

load of stories and roof is 200 kg/m^2; a load of walls of stories is 600 kg/m. To accurately specify seismic loads, the response modification factor (R) corresponding to the steel shear wall was determined based on the results of experimental tests conducted on the models of a concrete frame equipped with steel plate infill wall [28] and the considerations prescribed by ASCE-07 [35], and accordingly, it was chosen to be 7. To design thin SPSW, according to Canadian and American steel regulations, an equivalent brace is considered instead of each steel plate, and after calculating the cross-sectional area of each brace, the thickness of the steel plate is calculated from the following equation:

$$t = \frac{2A_b \sin\theta \cos 2\theta}{L \sin^2 2\alpha}, \tag{1}$$

where θ is the angle between the brace and the column, L is the span of the frame, A_b is the equivalent cross-sectional area of the brace, and α is the angle of formation of the diagonal tensile field in the steel plate After determining the thickness, each plate is converted into some diagonal strips, and the cross-section of each strip is obtained from the following equation:

$$A_s = \frac{L\cos\alpha + L\sin\alpha}{n} t, \tag{2}$$

where n is the number of bars. Numerous studies have been performed on the number of required strips, the results of which indicate the adequacy of 10 diagonal strips for the analysis of a thin shear steel shear wall. Given that the columns may buckle under the influence of the diagonal tensile field, the stiffness of the columns should be controlled by the following equation:

$$I_c \geq \frac{0.00307 t h_s^4}{L}, \tag{3}$$

where I_c is the moment of inertia of the columns, and h_s is story height. Also, to prevent the bending of the upper beam of the SPSW due to the effect of the asymmetric tensile field, equation (4) must be controlled:

$$M_{fpb} \geq \frac{\sigma_{ty} t L^2}{8} \sin^2 \alpha. \tag{4}$$

where M_{fpb} is the plastic anchor of the cross-section of the beam, and σ_{ty} is the final stress of the diagonal tensile field, which for thin plates is equal to their yield stress. Due to the small difference in the intensity of the diagonal tensile field between two adjacent stories, control of this relationship is required only for the end beam, but if the difference between the diagonal tensile fields between two adjacent stories is large, the relationship should be controlled for the middle beams.

For the records with different PGA intensities according to the Iranian earthquake standard 2800 regarding the comparison of the values of the acceleration response spectra of the earthquakes used in dynamic analysis with the values of the standard design spectrum, each sequence to reach 0.3 g was scaled. Steps 1 and 2 for the calculation of the scaling factor are as follows:

Step 1: scale each ground motion with the design spectural acceleration at the structure's fundamental period of vibration. This step results in a different scale factor, FPi, for each motion I, wherein the abbreviation FP refers to the fundamental period scaled motions.

Step 2: Individual scale factors are applied to the spectra such that the average of the scaled spectra does not fall below 1.0 times the design for any period between 0.2 T_1 and 1.5 T_1.

By applying the calculated scale factors, the models were nonlinear dynamic analysed, and request parameters were extracted.

In finally, the results were compared and concluded.

2.2. Modelling in OpenSees. For modeling, the beam and column elements (nonlinear beam-column) have been used. For modeling, SPSW strip method is used. In this method, initial imperfection of infill steel plate is not considered, and

Table 1: Comparison of finite element analysis results [29] and Choi and Park model test [28].

Lateral load (kN)			Elastic stiffness (kN/mm)			Energy dissipation (kN.m)		
Test	Finite element	Ratio finite element to test	Test	Finite element	Ratio finite element to test	Test	Finite element	Ratio finite element to test
886	903	1.02	53	48	0.91	323.98	349.23	1.08

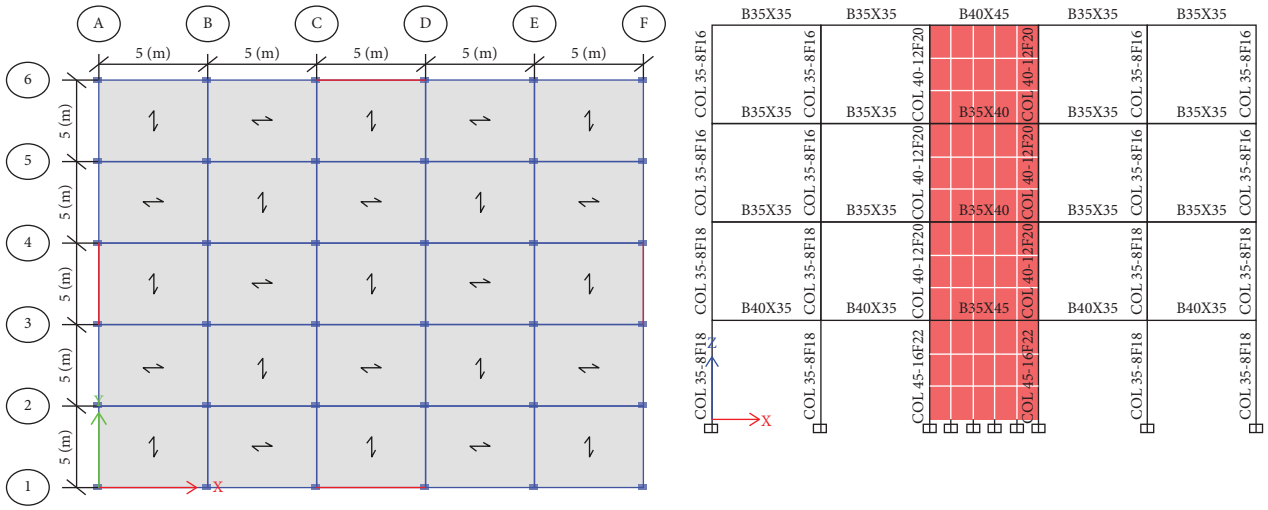

(a) (b)

Figure 3: (a) Plan of structural models. (b) 4-story model.

the tensile strip of the truss element is used. For the concrete and steel reinforcement materials, concrete02 and reinforcing steel materials can model the downward part of the performance curves that have been used for modeling concrete and steel materials of reinforcements, respectively. To model the actual behavior of the strips that should not react when pressed, hysteretic materials are used, which with the three-line behavior in tension and pressure gives the strips the property that does not show resistance when under pressure and allows that the diagonal tensile field of a SPSW is well modeled. When compression is applied to SPSW, using very low for example 1.e-20 for negative region, the truss model is modeling the behavior of SPSW in compression. OpenSees [29] uses the distributed plasticity by the fiber element. Regarding geometric nonlinearity, it should be said that the effects of geometric nonlinearity are defined by the transfer matrices that are a feature of OpenSees. In the mentioned program, after defining the geometry of the model, the gravitational analyses are gravitationally analysed (nonlinear static), and by setting the time in the amplitude of the problem to zero before performing the nonlinear dynamic analysis, the gravitational load values remain constant in subsequent dynamic analyses.

In the case of perimeter frames with considerable stiffness and accidental torsion relative to the middle frames, for the analysis of the structure designed in ETABS software, perimeter frames and their specifications have been used for two-dimensional nonlinear analysis. To take into account the effects of P-Δ, the leaning column method has been used. In this method, additional bays are defined. Columns between which are rotational springs with negligible stiffness with beams with high rigidity are connected to the main frame. The purpose of defining rotary springs with negativity is negligible so that the leaning columns do not absorb the momentum. Gravity loads are then applied to these columns. The interaction between soil and structure is not considered due to the relatively hard soil type and the fact that the dimensions of the structures and their foundations are not such that the propagation and return of the earthquake wave from the structure body to the soil are possible.

In the nonlinear dynamic analysis, the selection of a time interval of 30 seconds between the MS and AS with zero acceleration amplitude is considered to stabilize the frame under the effect of the MS excitation. This time interval has been selected based on analyses performed(Tables 6–8); in these Tables, predominant period of the records and period of damage of the models under seismic records were provided because the time gap relates to these periods. 5% damping was applied for all models.

To evaluate the seismic demands of RCF with SPSW, the parameters of peak maximum of drift demands and peak maximum displacement of stories and the maximum ductility and residual drift of stories have been selected to assess the seismic demand of models.

3. Nonlinear Static Analysis (Pushover) of RC and RC with SPSW

In order to compare the results of RCF equipped with SPSW with RCF, 4 structural models of RCF with the same plan as

Table 2: Properties of designed beams, columns, and steel plate shear walls of 4-story model (Figure 3(b)).

Story	Section columns of SPSW bay (cm)	Section beams of SPSW bay (cm)	Section columns of other bays (cm)	Section beams of other bays (cm) (width × height)	SPSW plate thickness (mm)
1	C45 × 45-16 ∅ 22	B 35 × 45	C 35 × 35-8 ∅ 18	B 35 × 40	1.6
2	C40 × 40-12 ∅ 20	B 35 × 40	C 35 × 35 -8 ∅ 18	B 35 × 35	1.6
3	C40 × 40-12 ∅ 20	B 35 × 40	C 35 × 35- 8 ∅ 16	B 35 × 35	1.6
4	C40 × 40-12 ∅ 20	B 45 × 40	C 35 × 35- 8 ∅ 16	B 35 × 35	1.1

Table 3: Properties of designed beams, columns, and steel plate shear walls of 8-story model.

Story	Section columns of SPSW bay (cm)	Section beams of SPSW bay (cm)	Section columns of other bays (cm)	Section beams of other bays (cm) (width × height)	SPSW plate thickness (mm)
1	C 80 × 80-32∅ 28	B 80 × 40	C 45 × 45-8 ∅ 18	B 45 × 50	2.1
2	C 80 × 80-32∅ 25	B 80 × 40	C 40 × 40-8 ∅ 18	B 45 × 50	2.1
3	C 75 × 75-28 ∅ 25	B 75 × 40	C40 × 40-8 ∅ 18	B 45 × 50	2.1
4	C 70 × 70-24 25	B 70 × 40	C45 × 45-8 ∅ 18	B 45 × 50	1.8
5	C 65 × 65-20∅ 22	B 65 × 40	C 40 × 40-8 ∅ 16	B 40 × 40	1.8
6	C 60 × 60-16 ∅ 20	B 60 × 40	C 40 × 40-8 ∅ 16	B 40 × 40	1.8
7	C 60 × 60-12∅ 18	B 60 × 40	C 40 × 40-8 ∅ 16	B 40 × 40	1.6
8	C 60 × 60-8 ∅ 18	B 60 × 60	C 35 × 35-8 ∅ 16	B 35 × 35	1.1

Table 4: Properties of designed beams, columns, and steel plate shear walls of 12-story model.

Story	Section columns of SPSW bay (cm)	Section beams of SPSW bay (cm)	Section columns of other bays (cm)	Section beams of other bays (cm) (width × height)	SPSW plate thickness (mm)
1	C 95 × 95-52 ∅ 32	B 95 × 55	C 50 × 50-16 ∅ 20	B 50 × 55	2.1
2	C 95 × 95-52 ∅ 32	B 95 × 55	C 50 × 50-12 ∅ 20	B 50 × 55	2.1
3	C 95 × 95-48∅ 28	B 95 × 55	C 45 × 45-12 ∅ 20	B 45 × 55	2.1
4	C 90 × 90-48∅ 28	B 90 × 50	C 45 × 45-12 ∅ 20	B 45 × 50	2.1
5	C 85 × 85-40 ∅ 28	B 85 × 50	C 45 × 45-12 ∅ 20	B 45 × 50	1.8
6	C 80 × 80-24∅ 28	B 80 × 50	C 45 × 45-12∅ 20	B 45 × 50	1.8
7	C 75 × 75-24 ∅ 25	B 75 × 45	C 40 × 40-12 ∅ 20	B 40 × 45	1.8
8	C 70 × 70-24 ∅ 20	B 70 × 45	C 40 × 40-12 ∅ 20	B 40 × 45	1.8
9	C 65 × 65-16∅ 20	B 65 × 45	C 40 × 40-8 ∅ 20	B 40 × 45	1.6
10	C 60 × 60-12∅ 20	B 60 × 40	C 35 × 35-8 ∅ 20	B 35 × 40	1.6
11	C 60 × 60-12 ∅ 20	B 60 × 40	C 35 × 35-8 ∅ 18	B 35 × 40	1.36
12	C 60 × 60-12 ∅ 20	B 60 × 60	C 35 × 35-8 ∅ 18	B 35 × 40	1.1

in Figure 3(a) were designed with high ductility and modeled in OpenSees software. Nonlinear static analysis (Pushover) of models was performed in OpenSees finite element software [29].

3.1. Lateral Load Distribution in Pushover Analysis. Upon the Iranian 2800 earthquake standard, lateral seismic force at level x, Fx, shall be calculated from the following equation:

$$Fx = CvxVu, \tag{6}$$

where

$$C_{vx} = \frac{w_X {h_x}^k}{\sum_{i=1}^{n} w_i {h_i}^k}, \tag{7}$$

where C_{vx} = vertical distribution factor, w_x = the portion of the effective seismic weight assigned to level i or x, h_x = height of level i or x, calculated from base level, n = number of stories (levels), k = distribution exponent related to the structure period determined from the following equation:

$$K = \begin{cases} 1 & T \le 0.5 \\ 0.5T + 0.75 & 0.5 < T < 2.5 \\ 2 & T \ge 2.5 \end{cases}. \tag{8}$$

The results of this analysis were shown in Figures 4–7. In these figures, the vertical axis is shown as the ratio of base shear (V) to weight models that represented coefficient base shear in the Iranian 2800 earthquake standard [34], and axis horizontal is shown drift ratio of the highest models. Shear forces for design basis earthquake (DBE) and maximum considered earthquake (MCE) were calculated and presented in the two last columns of Table 9.

As shown in Figure 4, 4-story model (RC with SPSW) has a stiffness greater than 8 story up 1.8 times (Table 9), 8-story model has a stiffness greater than 12 story up 1.08 times (Table 9), and 12-story model has a stiffness greater than 24 story up 1.5 times (Table 9). As shown in Figures 5–7, 4-story model (RC with SPSW) has a stiffness greater than 4-story

Table 5: Properties of designed beams, columns, and steel plate shear walls of 24-story model.

Story	Section columns of SPSW bay (cm)	Section columns of adjacent SPSW (cm)	Section columns of other bays (cm)	Section beams of SPSW and external bays (cm)	Section beams of adjacent SPSW (cm)	Plate thickness of SPSW (mm)
1	C 105 × 105-25 ∅ 52	C 80 × 80-25 ∅ 32	C 80 × 80-25 ∅ 24	B 70 × 70	B 65 × 65	4.4
2	C 100 × 100-25 ∅ 48	C 80 × 80-25 ∅ 28	C 80 × 80-20 ∅ 24	B 70 × 70	B 65 × 65	3.2
3	C 95 × 95-25 ∅ 44	C 80 × 80- 25 ∅ 28	C 80 × 80-20 ∅ 24	B 70 × 70	B 65 × 65	3.2
4	C 90 × 90-25 ∅ 40	C 75 × 75–25 ∅ 28	C 75 × 75-20 ∅ 24	B 70 × 70	B 65 × 65	3.2
5	C 90 × 90-25 ∅ 40	C 75 × 75–25 ∅ 28	C 75 × 75-20 ∅ 24	B 70 × 70	B 65 × 65	3.2
6	C-80 × 80-25 ∅ 36	C 70 × 70-25 ∅ 28	C 70 × 70-20 ∅ 24	B 70 × 70	B 65 × 65	3.2
7	C 80 × 80-25 ∅ 48	C 70 × 70-20 ∅ 24	C 70 × 70-20 ∅ 24	B 70 × 70	B 65 × 65	3.2
8	C 80 × 80-25 ∅ 28	C 70 × 70-20 ∅ 24	C 70 × 70-20 ∅ 20	B 70 × 70	B 65 × 65	3.2
9	C 75 × 75-25 ∅ 28	C 70 × 70-20 ∅ 24	C 70 × 70-20 ∅ 20	B 70 × 70	B 65 × 65	2.9
10	C 75 × 75-25 ∅ 24	C 70 × 70-20 ∅ 24	C 710 × 70-20 ∅ 20	B 60 × 60	B 55 × 55	2.9
11	C 70 × 70-25 ∅ 24	C 65 × 65-20 ∅ 24	C 65 × 65-20 ∅ 16	B 60 × 60	B 55 × 55	2.9
12	C 65 × 65-25 ∅ 24	C 60 × 60-20 ∅ 24	C 60 × 60-18 ∅ 16	B 60 × 60	B 55 × 55	2.9
13	C 65 × 65-25 ∅ 24	C 60 × 60-20 ∅ 24	C 60 × 60-18 ∅ 16	B 60 × 60	B 55 × 55	2.9
14	C 60 × 60-25 ∅ 24	C 55 × 55-20 ∅ 24	C 55 × 55-18 ∅ 16	B 50 × 50	B 50 × 50	2.9
15	C 55 × 55-20 ∅ 24	C 55 × 55-20 ∅ 24	C 55 × 55-18 ∅ 16	B 50 × 50	B 50 × 50	2.9
16	C 55 × 55-18 ∅ 24	C 50 × 50-18 ∅ 24	C 50 × 50-12 ∅ 18	B 50 × 50	B 50 × 50	2.6
17	C 50 × 50-18 ∅ 24	C 50 × 50-18 ∅ 24	C 50 × 50-12 ∅ 18	B 50 × 50	B 50 × 50	2.1
18	C 50 × 50-18 ∅ 24	C 45 × 45-18 ∅ 24	C 45 × 45-12 ∅ 16	B 50 × 50	B 50 × 50	2.1
19	C 45 × 45-18 ∅ 24	C 45 × 45-18 ∅ 24	C 45 × 45-12 ∅ 18	B 50 × 50	B 50 × 50	1.8
20	C 45 × 45-18 ∅ 24	C 45 × 45-18 ∅ 24	C 45 × 45-12 ∅ 18	B 50 × 50	B 50 × 50	1.8
21	C 40 × 40-18 ∅ 20	C 40 × 40-18 ∅ 20	C 40 × 40-12 ∅ 16	B 40 × 40	B 40 × 40	1.6
22	C 40 × 40-18 ∅ 20	C 40 × 40-18 ∅ 20	C 40 × 40-12 ∅ 16	B 40 × 40	B 40 × 40	1.6
23	C 40 × 40-18 ∅ 18	C 40 × 40-18 ∅ 16	C 40 × 40-12 ∅ 16	B 40 × 40	B 40 × 40	1.36
24	C 40 × 40-18 ∅ 18	C 40 × 40-18 ∅ 16	C 40 × 40-12 ∅ 16	B 60 × 40	B 40 × 40	1.1

Table 6: The first-mode period of vibration and period of damaged of the models under Group I.

Earthquake model	Chalfant Valley		Hollister		New Zealand	
	$T_1(s)$	TD (s)	$T_1(s)$	TD (s)	$T_1(s)$	TD (s)
4 (RCF + SPSW)	0.32	0.35	0.32	0.36	0.32	0.42
8 (RCF + SPSW)	0.63	0.71	0.63	0.72	0.63	0.91
12 (RCF + SPSW)	0.88	1.12	0.88	1.12	0.88	1.18
24 (RCF + SPSW)	1.56	2.04	1.56	2.11	1.56	1.86
4 (RCF)	0.78	1.38	0.78	1.51	0.78	1.31
8 (RCF)	0.81	1.36	0.81	1.39	0.81	1.36
12 (RCF)	1.29	2.32	1.29	1.81	1.29	1.77
24 (RCF)	1.76	2.41	1.76	2.88	1.76	2.21

Table 7: The first-mode period of vibration and period of damaged of the models under Group II.

Earthquake model	Chalfant Valley		Chi-Chi Taiwan 1		Chi-Chi Taiwan 2		Imperial Valley		Irpinia, Italy 1		Irpinia, Italy 2		Northridge 1		Northridge 2	
	$T_1(s)$	TD (s)	$T_1(s)$	TD (s)	$T_1(s)$	TD (s)	$T_1(s)$	TD (s)	$T_1(s)$	TD (s)	$T_1(s)$	TD (s)	$T_1(s)$	TD (s)	$T_1(s)$	TD (s)
4 (RCF + SPSW)	0.32	0.34	0.32	0.35	0.32	0.36	0.32	0.35	0.32	0.35	0.32	0.35	0.32	0.5	0.32	0.41
8 (RCF + SPSW)	0.63	0.71	0.63	0.68	0.63	0.69	0.63	0.72	0.63	0.72	0.63	0.75	0.63	0.88	0.63	0.93
12 (RCF + SPSW)	0.88	1.12	0.88	1.02	0.88	1.08	0.88	1.11	0.88	1.13	0.88	1.12	0.88	1.17	0.88	1.10
24 (RCF + SPSW)	1.56	2.06	1.56	1.86	1.56	2.08	1.56	2.14	1.56	2.18	1.56	1.82	1.56	2.08	1.56	2.09
4 (RCF)	0.78	1.46	0.78	1.21	0.78	1.38	0.78	1.43	0.78	1.53	0.78	1.56	0.78	1.51	0.78	1.45
8 (RCF)	0.81	1.35	0.81	1.16	0.81	1.34	0.81	1.33	0.81	1.35	0.81	1.40	0.81	1.38	0.81	1.35
12 (RCF)	1.29	1.62	1.29	2.03	1.29	2.31	1.29	2.17	1.29	2.31	1.29	2.0	1.29	2.3	1.29	2.25
24 (RCF)	1.76	2.23	1.76	3.04	1.76	3.05	1.76	3.24	1.76	2.73	1.76	2.19	1.76	2.97	1.76	2.97

Table 8: The first-mode period of vibration and period of damaged of the models under group III.

Earthquake model	Imperial Valley		Coalinga		Chalfant Valley		Whittier	
	T_1 (s)	TD (s)	T_1 (s)	TD (s)	T1(s)	TD (s)	T_1 (s)	TD (s)
4 (RCF + SPSW)	0.32	0.35	0.32	0.34	0.32	0.35	0.32	0.35
8 (RCF + SPSW)	0.63	0.71	0.63	0.69	0.63	0.69	0.63	0.73
12 (RCF + SPSW)	0.88	1.12	0.88	1.07	0.88	1.07	0.88	1.12
24 (RCF + SPSW)	1.56	2.13	1.56	2.12	1.56	1.91	1.56	2.13
4 (RCF)	0.78	1.49	0.78	1.35	0.78	1.22	0.78	1.47
8 (RCF)	0.81	1.38	0.81	1.35	0.81	1.23	0.81	1.38
12 (RCF)	1.29	2.09	1.29	2.30	1.29	2.0	1.29	2.33
24 (RCF)	1.76	3.26	1.76	3.07	1.76	2.91	1.76	2.96

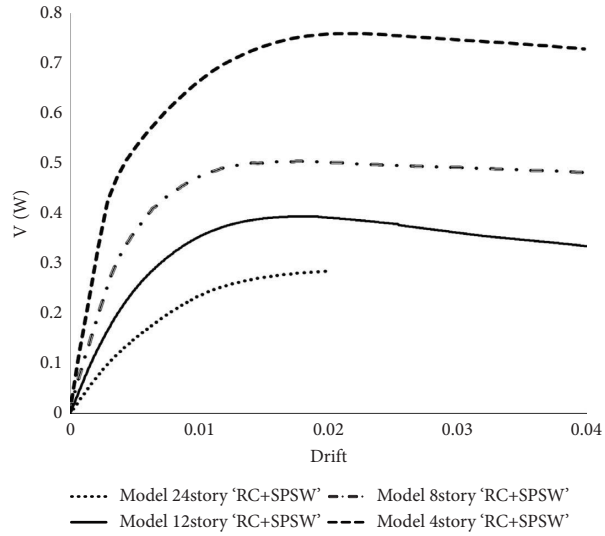

Figure 4: Result of nonlinear static analysis of models.

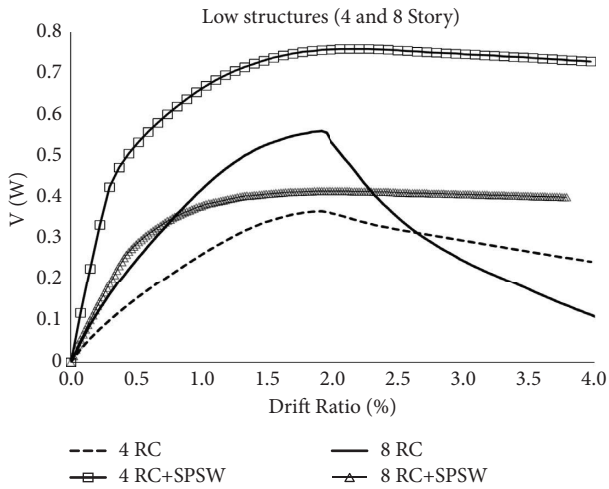

Figure 5: Result of nonlinear static analysis of low-rise structures.

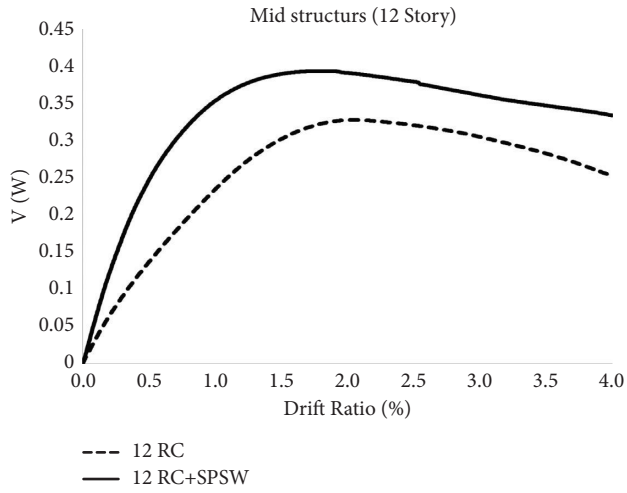

Figure 6: Result of nonlinear static analysis of mid-rise structures.

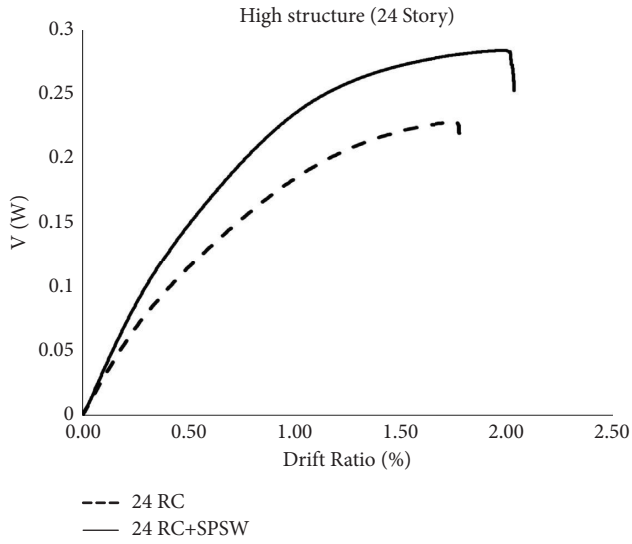

Figure 7: Result of nonlinear static analysis of high-rise structures.

model (RC without SPSW) up 3.12 times (Table 9), 8-story model (RC with SPSW) has stiffness greater than 8-story model (RC without SPSW) up 1.05 times (Table 9), 12-story model (RC with SPSW) has stiffness greater than 12-story model (RC without SPSW) up 1.50 times (Table 9), and 24-story model (RC with SPSW) has stiffness greater than 24-story model (RC without SPSW) up 1.23 times (Table 9).

3.2. Selected Seismic Records in Nonlinear Dynamic Analysis. Seismic sequences (SS) have been applied to the models in 2 ways, including real seismic records and artificial seismic. In the real seismic method, using the sequence seismic records recorded in the recorded stations and the artificial method due to the unavailability of an insufficient number of sequence real seismic records, an artificial AS has been applied to the models. Considering a few sequence seismic records in different seismic areas of the world, to investigate the effects of this event on the performance of structures with different construction conditions and also for a more realistic investigation of the effect of sequence seismic on the performance of structures, the need to use artificial seismic is more felt [36]. According to studies, the most important approaches to the production of artificial seismic records using the real seismic record are the back-to-back (repetitive) approach and the randomized approach [36, 37].

In the method of real seismic, three groups of seismic records including records of real MS with maximum effective peak acceleration (EPA) and their AS records (Group I), real MS records with nearly maximum EPA and their AS records (Group II), real seismic records with PGA (AS to MS) greater than 1.0 [16] (Group III) have been used, and in the method of artificial seismic, some important seismic records (the far and near-field) are studied in the form of seismic scenarios.

3.3. Real Seismic Records with Maximum EPA (Group I). These records have been selected based on the Ruz-Garcia in 2012 [36] and Amiri and Dana study in 2005 [38] in which the effective peak acceleration (EPA) parameter is included. The definition of the EPA parameter, which is similar to the maximum PGA ground acceleration of the acceleration type, is equal to the divided average spectral acceleration of an earthquake with 5% damping over a while of 0.1 seconds to 0.5 seconds by the standard magnification factor of 2.5. EPA is like the peak ground acceleration PGA of the acceleration type. For selecting the critical seismic scenario parameters such as peak ground acceleration (PGA), effective peak acceleration (EPA), peak ground velocity (PGV), peak ground displacement (PGD), duration Earthquake and Arias intensity(The definition of Arias intensity is the sum of total energy per unit weight in a system of one degree of non-damping freedom that has frequencies with uniform distribution from zero to infinity, and in this research it has been used to calculate the effective duration of earthquakes) have been considered. These parameters due to having the highest correlation with other parameters have been introduced as the most appropriate criterion for selecting the most critical scenario [38]. In such a way, the mentioned records are more critical in terms of the impact on the behavior of the structure and its response than other sequence seismic records recorded in other stations. The reason for using the records presented in this research is to avoid creating uncertainties in introducing the characteristics of the following earthquakes by using artificial methods and sometimes proposed models based on Gutenberg-Richter, Amory, and Beth's laws. Thus, in all selected scenarios from the PEER database, the magnitude, duration, time interval between sequence seismic records, and other seismic properties are real. The conditions for selecting sequence real earthquakes used in this paper, in addition to the fact that the recording stations of the first and second earthquakes are the same and the time interval between them is less than ten minutes, are the discussion of the effective peak acceleration of these earthquakes. So that, in the sequence seismic records shown in Table 10, both the first earthquake and the second earthquake have an EPA among the other records recorded for the desired earthquake.

Table 9: Summary of calculation models' ductility and stiffness.

Lateral bearing system	Model	T_1 (s)	D_y (cm)	D_{max} (cm)	V_y (T)	$\mu = D_{max}/D_y$	$K_y = V_y/D_y$ (T/cm)	V_{DBE} (T)	V_{MCE} (T)
RCF + SPSW	4-Story	0.32	7	35	198	5.0	28.29	29.72	30.61
RCF + SPSW	8-Story	0.63	18	81	285	4.5	15.8	62.82	65.96
RCF + SPSW	12-Story	0.88	28	163	408	5.82	14.6	84.38	87.76
RCF + SPSW	24-Story	1.56	40	163	496	4.08	12.4	132	135.96
RCF	4-Story	0.78	13	35	118	2.69	9.07	31.82	32.67
RCF	8-Story	0.81	12	50	180	4.17	15	44.59	46.28
RCF	12-Story	1.29	26	76	253	2.92	9.73	91.5	94.89
RCF	24-Story	1.76	42	135	424	3.21	10.10	153	158.51

The first fundamental period of 4-, 8-, 12-, and 24-story models (T_1) is 0.32, 0.63, 0.88, and 1.56 seconds, respectively. According to the unit design for records with different PGA intensities and the Iranian earthquake standard 2800 [34] regarding the comparison of the values of the acceleration response spectra of the earthquakes used in dynamic analysis with the values of the standard design spectrum, each sequence to reach 0.3 g was scaled. The method for scaling earthquakes according to the standard of 2800 Iranian earthquakes is the same as in ASCE7-2010. For the high-rise building (24 stories) with the first fundamental period greater than 1 second, the design spectrums of the [34] modification coefficient are equal to 1.104 for the soil type III. The calculated scale factors of earthquakes for each model are presented in the last column of Tables 10 and 11.

3.4. Real Seismic Records (Seismic Records with Nearly Maximum EPA) (Group II). Due to the limited number of selected records, a sequential seismic scenario called with nearly maximum EPA (Table 11) is considered, in which the first or second earthquake is ranked second or final third in terms of the amount of EPA relative to the maximum. With these considerations, 11 sequence records introduced in Tables 10 and 11 records have been selected for nonlinear dynamic analysis.

3.5. Real Seismic Records with PGA (AS to MS) Greater than 1.0 (Group III). Four records of earthquakes are used by researchers [16, 39] as their MS and AS are presented in Table 12.

3.6. Artificial Seismic MS and AS (Near-Field and Far-Field) (Seismic Scenario) (Group IV). As shown in Tables 13 and 14, SS (the first 4 records of the far-field and the second 4 records of the near-field) is presented artificially to apply back-to-back and randomized methods with different AS.

3.7. Effective Characteristics of Earthquakes in the Structural Response. In nonlinear time history analysis, the behavior of the structure is observed during the earthquake time, and this analysis shows the more realistic behavior of the structure during the earthquake compared to other analyses. In this type of analysis, the effect of peak ground acceleration (PGA), frequency content, and time of the earthquake (effective duration of the earthquake) is well observed. In this study, to investigate the effect of PGA, a relatively wide range of the ratio of PGA AS to a MS of strong earthquakes has been considered. These ratios are 0.04, 0.18, 0.21, 0.28, 0.32, 0.38, 0.43, 0.46, 0.74, 0.97, and 1.23 for real seismic records of groups I and II and 1.06, 1.15, 1.30, and 1.89 for accelerometers of group III. Peak ground motions have a greater effect on the amplitude of vibrations. If the frequency content of the earthquake and vibration frequencies of the structure is close, the earthquake will cause the greatest amplification in the structure. The frequency content is reflected in the acceleration response spectrum or the Fourier spectrum of its acceleration amplitude. The predominant period of earthquakes (Tg) was obtained using SeismoSignal [40, 41]. Research shows that the PGA of earthquakes alone is not a good quantity to determine the earthquake effects. The damage caused by an earthquake is related to the amount of energy of the earthquake movements in a building.

The duration of the earthquake in most cases has a significant effect on the inelastic deformation of the structure and therefore in determining the amount of input energy to the structure, linear, and nonlinear analysis of the structural response and also in the statistical method of determining the structure's response to an earthquake is widely used. There are different methods for determining the duration of an earthquake using the characteristics and effective parameters of seismic acceleration. One of these methods is Trifunac and Brady method, which has defined the period of strong vibration as the time interval in which a significant contribution is added to the square integral of the accelerations, called the acceleration intensity. They have chosen the time interval between the 5% and 95% stocks as the period of strong. In this research, the effective duration of earthquakes was obtained using SeismoSignal [40] and was used in the nonlinear dynamic analysis of models.

4. Seismic Demands of Models under MS and SS

4.1. Seismic Demands of Models under MS and SS Group I (Maximum EPA). Models were analysed nonlinear dynamic time history under MS of group I (Figure 8). Parameters of peak displacement demand, peak maximum interstory drift demand, and maximum ductility demand were extracted.

The displacement response of the 4-story model with the vibration period of the first mode 0.32 sec due to proximity to the frequency content of the New Zealand main-shock (0.38 sec) (Table 14) was resonanced (Figure 9(a)).

Table 10: Result for scaling the first category records of seismic scenario (with maximum EPA).

MS-AS	Station name	Date time	Arias intensity cm/s	PGA (g) MS	PGA (g) AS	Ratio PGA AS to MS	EPA (MS, AS)	Scale coefficient (RCF + SPSW)			
								4st	8st	12st	24st
Chalfant Valley	CDMG 54428 Zack Brothers Ranch	86-07-21 14 : 42, 14 : 51	193.3 11	0.446	0.143	0.32	0.4854, 0.1047	0.67	0.78	0.89	1.16
Hollister	USGS 1028 Hollister city Hall	61-04-09 7 : 23, 7 : 5	13.3 9.6	0.074	0.072	0.97	0.0725, 0.0794	4.70	4.10	4.32	5.36
New Zeland	99999 Matahina Dam	87-03-02 1 : 42, 1 : 51	65.2 2.6	0.255	0.053	0.21	0.2601, 0.043	1.23	1.50	1.69	2.19

Table 11: Result for scaling the second category of seismic scenario (with nearly maximum EPA).

MS-AS	Station name	Date time	Arias intensity cm/s	PGA (g) MS	PGA (g) AS	Ratio PGA AS to MS	EPAMS, AS	Scale coefficient (RCF + SPSW)			
								4st	8st	12st	24st
Chalfant Valley	CDMG 54171 Bishop-LADWP South St	86-07-21 14 : 42, 14 : 51	50.1 6.9	0.248	0.106	0.43	0.2197, 0.0887	1.37	1.65	1.83	2.70
Chi-Chi Taiwan 1	CWB 99999 TCU079	99-09-20 17 : 57, 18 : 03	31.7 63.9	0.212	0.262	1.23	0.1797, 0.2268	1.31	1.78	2.15	4.17
Chi-Chi Taiwan 2	CWB 99999 TCU129	99-09-20 17 : 57, 18 : 03	14.8 78.7	0.396	0.15	0.38	0.1026, 0.2844	1.00	1.42	1.72	3.73
Imperial Valley	USGS 952 EL Centro Array #5	79-10-15 23 : 16, 23 : 19	165.4 11.1	0.519	0.238	0.46	0.421, 0.1614	0.71	0.92	1.05	1.28
Irpinia, Italy 1	ENEL 99999 Sturno	80-11-23 19 : 34, 19 : 35	144.1 7.3	0.25	0.071	0.28	0.2528, 0.0771	1.29	1.35	1.46	1.37
Irpinia, Italy 2	ENEL 99999 Calitri	80-11-23 19 : 34, 19 : 35	57.8 46.3	0.177	0.132	0.74	0.1335, 0.1221	2.43	2.28	1.69	1.82
Northridge 1	CDMG 24279 Newhall–Fire Sta	94-01-17 12 : 31, 12 : 32	436 1.3	0.583	0.107	0.18	0.6244, 0.0385	0.49	0.58	0.62	0.78
Northridge 2	CDMG 24436 Tarzana–Cedar Hill A	94-01-17 12 : 31, 12 : 41	2274.8 4.5	1.78	0.069	0.04	1.3491,.0638	0.22	0.28	0.34	0.47

Therefore, the role of frequency content in the behavior and response of the 4-story model is well evident. Also, in the 8-story model, the role of frequency content is well represented by the displacement response of the stories under the New Zealand main-shock (Figure 9(b)).

The effective parameters involved in estimating the seismic demands of the models, including the ratio PGA of AS to MS the frequency content, predominant period, damage period of the models at the end of MS (Table 6), have been investigated. Comparison of the first mode period of vibration and period of damaged (TD) of the low-rise of RCF with SPSW under MS and AS of group I (Table 12) shows that this model except New Zealand MS in other MS, the first mode period of vibration of models closed to damage period

Table 12: Real seismic records with PGA (AS to MS) greater than 1.0 [16, 39].

NO	MS-AS	RSN	Magnitude	Arias (cm/s) intensity	PGA (g)
1	Chalfant Valley	547	5.77	53.7	0.236
	Chalfant Valley	558	6.19	193.8	0.447
2	Coalinga	406	5.77	82.8	0.519
	Coalinga	418	5.21	142.4	0.677
3	Imperial Valley	185	6.53	86	0.221
	Imperial Valley	208	5.01	13.5	0.255
4	Whittier	691	5.99	30.5	0.194
	Whittier	716	5.27	17.5	0.206

Table 13: Seismic MS and AS records (near-field and far-field) (SS).

NO	Earthquake	RSN	Arias intensity (cm/s)	Magnitude	PGA (g)
1	Tabas	140	21.5	7.35	0.1049
2	Trinidad	280	17.2	7.2	0.1474
3	Taiwan Smart1	425	2	6.5	0.02825
4	Northridge-01	943	7.4	6.69	0.0673
5	Loma Prieta	764	72.1	6.93	0.2853
6	Kobe	1116	63.9	6.9	0.233
7	Northridge-06	1739	94.5	5.28	0.373
8	Parkfield	4125	10.4	6	0.103

Table 14: Parameters and effective characteristics in the response of models under Group I.

Earthquake parameter	Chalfant Valley		Hollister		New Zealand	
	MS	AS	MS	AS	MS	AS
PGA (g)	0.446	0.143	0.074	0.072	0.255	0.053
PGA as/PGAms	0.32		0.97		0.21	
Tg (s)	0.2	0.12	0.48	0.32	0.38	0.28
Tg, AS/Tg, MS	0.6		0.67		0.74	
tDs	6.17	7.64	19.10	16.87	6.22	10.66

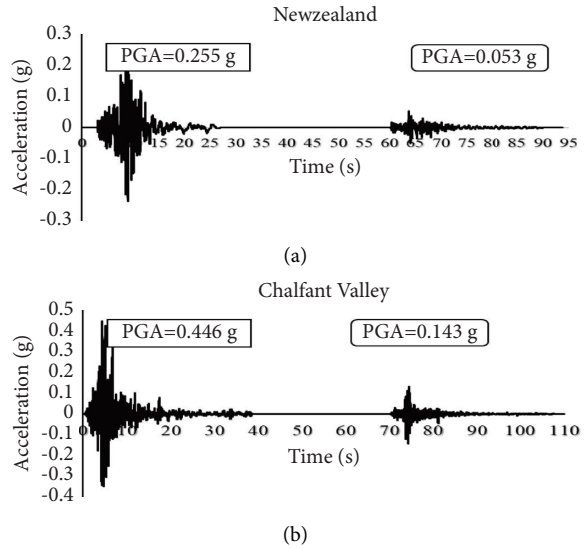

Figure 8: SS records with maximum EPA: (a) New Zealand accelerometer. (b) Chalfant Valley accelerometer.

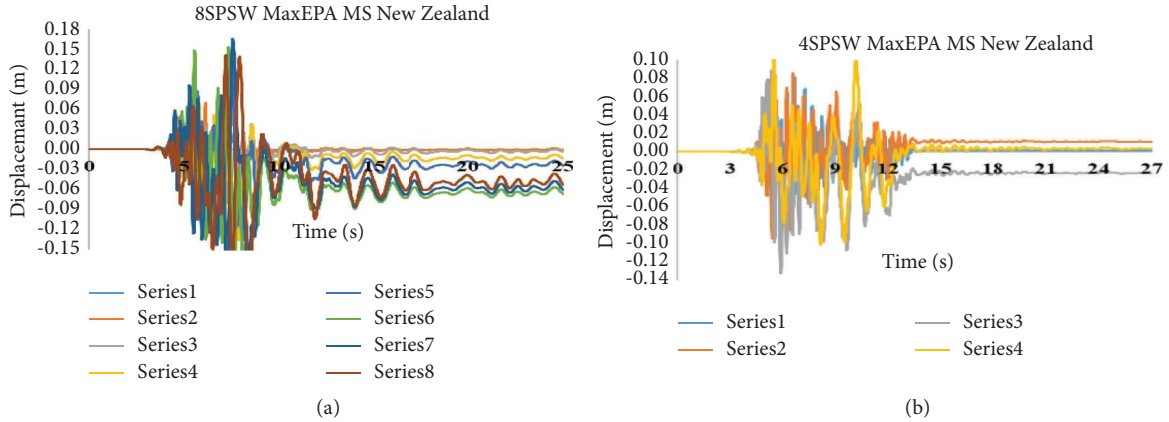

Figure 9: Time history of the displacement response under New Zealand MS: (a) 4-story model, (b) 8-story model.

Table 15: Results of peak maximum interstory drift demand of models in the MS and SS Group I.

Earthquake model	Chalfant Valley (%)		Hollister		New Zealand	
	SS (%)	MS (%)	MS (%)	SS (%)	MS (%)	SS (%)
4 (RCF + SPSW)	0.4	1.01	0.55	0.63	1.65	1.65
8 (RCF + SPSW)	0.48	0.48	0.5	0.5	1.07	1.07
12 (RCF + SPSW)	0.73	0.73	0.65	0.65	1.76	1.76
24 (RCF + SPSW)	0.9	1.29	1.30	1.59	1.51	1.51
4 (RCF)	1.35	1.56	1.96	2.10	1.66	1.66
8 (RCF)	0.94	0.94	0.95	0.99	1.11	1.11
12 (RCF)	1.65	1.65	1.88	1.88	1.75	1.75
24 (RCF)	1.76	1.76	1.98	1.98	1.76	1.76

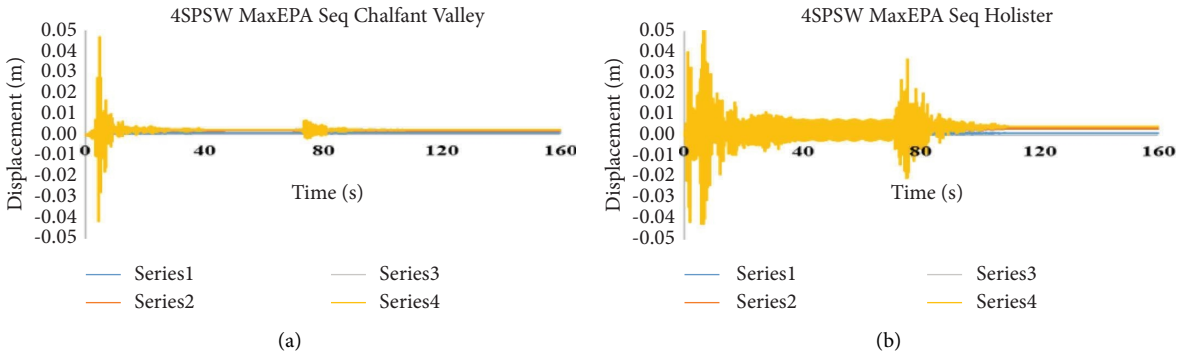

Figure 10: Time history response of 4-story model (RC + SPSW) under SS: (a) Chalfant Valley. (b) Hollister.

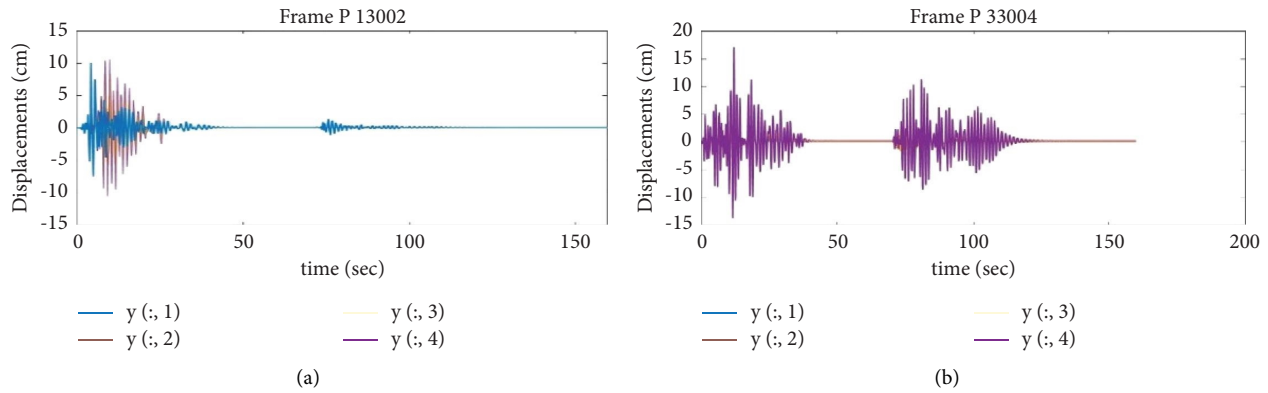

Figure 11: Time history response of 4-story model (RC) under SS: (a) Chalfant Valley. (b) Hollister.

Table 16: Results of residual drift analysis of models under MS and SS of seismic scenario with maximum EPA.

Earthquake model	Chalfant Valley		Hollister		New Zealand	
	MS (%)	SS (%)	MS (%)	SS (%)	MS (%)	SS (%)
4 (RCF + SPSW)	0.016	−0.06	−0.08	0.03	−0.2	−0.2
8 (RCF + SPSW)	0.01	0.01	−0.06	−0.01	−0.32	−0.32
12 (RCF + SPSW)	−0.01	0.01	0.012	0.002	0.14	0.14
24 (RCF + SPSW)	−0.01	0.04	−0.01	−0.01	0.08	0.08
4 (RCF)	0.04	0.01	0.03	0.02	−0.07	0.03
8 (RCF)	0.01	0.004	−0.004	0.001	−0.004	0.001
12 (RCF)	0	−0.002	−0.088	−0.002	0.145	0.002
24 (RCF)	0.07	0.025	0.06	0.05	0.11	0.005

Table 17: Parameters and effective characteristics in the response of models under Group II (nearly maximum EPA).

Earthquake parameter	Chalfant Valley		Chi-Chi Taiwan 1		Chi-Chi Taiwan 2		Imperial Valley		Irpinia, Italy 1		Irpinia, Italy 2		Northridge 1		Northridge 2	
	MS	As	MS	As	MS	As	MS	As	MS	As	MS	As	MS	As	MS	As
PGA (g)	0.248	0.106	0.212	0.262	0.396	0.15	0.519	0.238	0.25	0.071	0.177	0.132	0.58	0.107	1.78	0.069
PGA as/PGAms	0.43		1.23		0.38		0.46		0.28		0.74		0.18		0.04	
Tg (s)	0.24	0.22	0.2	0.24	0.16	0.2	0.34	0.24	0.44	0.22	0.48	1.16	0.32	0.28	0.32	0.26
Tg, AS/Tg, MS	0.92		1.2		1.25		0.71		0.5		2.42		0.88		0.81	
tD (s)	12.57	13.85	4.72	14.5	10.25	14.09	8.25	6.96	18.21	14.07	23.34	19.01	5.88	12.48	10.54	12.92

Table 18: Results of peak interstory drift demand of models in the MS and SS for earthquakes Group II.

Earthquake model	Chalfant Valley		Chi-Chi Taiwan 1		Chi-Chi Taiwan 2		Imperial Valley		Irpinia, Italy 1		Irpinia, Italy 2		Northridge 1		Northridge 2	
	MS (%)	SS (%)	MS (%)	SS (%)	MS (%)	SS (%)	MS (%)	SS (%)	MS (%)	SS (%)	MS (%)	SS (%)	MS (%)	SS (%)	MS (%)	SS (%)
4 (RCF + SPSW)	0.26	0.26	0.36	0.32	0.48	0.48	0.31	0.31	0.52	0.86	0.4	0.4	4.9	4.9	5.1	5.1
8 (RCF + SPSW)	0.47	0.47	0.24	0.27	0.35	0.31	0.53	0.53	0.58	0.64	0.96	1.28	2.82	2.82	4.25	4.25
12 (RCF + SPSW)	0.4	0.7	0.4	0.48	0.4	0.6	0.6	0.65	0.56	0.7	1.01	1.02	2.01	2.01	0.79	0.79
24 (RCF + SPSW)	1.23	1.4	0.81	1.2	0.69	1.5	1.31	1.5	0.6	1.31	0.64	0.78	0.54	1	1.34	1.9
4 (RCF)	1.79	1.79	0.82	1.14	0.89	0.93	1.32	1.32	1.81	1.81	2.17	2.34	1.89	1.89	1.50	1.50
8 (RCF)	0.81	0.81	0.70	0.72	0.63	0.71	0.98	0.98	1.09	1.09	1.58	2.28	0.98	0.98	0.82	0.82
12 (RCF)	2.03	2.03	1.36	1.91	1.75	2.19	2.24	2.24	1.57	1.57	1.86	1.86	1.57	1.57	2.0	2.0
24 (RCF)	2.2	2.2	2.56	2.56	3.03	3.03	2.45	2.45	2.07	2.07	1.83	1.83	3.20	3.20	2.0	2.0

that this implies the stiffness of this system was not reduced. In the mid- and high-rise structures, damaged period approximates up to 1.5 times the first-mode period of vibration. As shown in Table 15, the peak maximum interstory drift demand of the models under MS and SS is presented for comparison.

As shown in Table 13, in RCF with SPSW system, the results of peak maximum interstory drift demand of the models under the MS and SS of group I in the 4-story model, Chalfant Valley SS was increased peak maximum interstory drift demand greater than 2.5 times in MS demand. The peak maximum interstory drift demand of models 8 and 12 stories under any SS was constant, but in the 24-story model, this demand except New Zealand SS was increased in other SS. In the RCF system, SS in models 8, 12, and 24 story was not increased the peak maximum interstory drift demand, but in the 4-story model, this demand in all SS was increased.

The residual drifts of the models under MS and SS are presented in Table 16. As shown, the 4- and 8-story models have a residual drift of 0.2% and 0.32% in New Zealand MS that is related to content frequency of modes and New Zealand earthquake. The 9th story of the 12-story model in the New Zealand earthquake, entering the nonlinear area, caused a residual drift of 0.14%. From Table 16, it can be considered that AS in some of group I changed the magnitude and direction of residual drift, and in some others, earthquakes remained constant.

4.2. Seismic Demands of Models under MS and SS Group II (Nearly Maximum EPA). The 4-story model with RCF with SPSW, the first-mode period of vibration of 0.32 seconds, is close to the frequency content of Northridge1 and Northridge2 MS with a predominant period of 0.32 seconds (Table 7). In other earthquakes of this group, this model has a predominant period greater or less than the first-mode period of vibration of the models and has no response to displacement of the increased stories. The 12-story model with RCF with SPSW, the

Table 19: Results of residual drift (%) analysis of models under MS and SS of seismic scenario with nearly maximum EPA.

Earthquake model	Chalfant Valley		Chi-Chi Taiwan 1		Chi-Chi Taiwan 2		Imperial Valley		Irpinia, Italy 1		Irpinia, Italy 2		Northridge 1		Northridge 2	
	MS	SS	MS	SS	MS	SS	MS	SS	MS	SS	MS	SS	MS	SS	MS	SS
4 (RCF + SPSW)	0.12	0.1	0.001	0.001	0.007	−0.003	0.001	0.003	−0.017	−0.04	−0.018	−0.017	−2.4	−2.4	−0.25	−0.25
8 (RCF + SPSW)	0.01	0.01	−0.003	−0.003	−0.008	0.0002	−0.01	−0.01	0.03	0.03	0.05	−0.03	−0.31	−0.31	0.8	0.8
12 (RCF + SPSW)	0.01	0.01	0.008	0.007	−0.002	0.004	0.02	0.018	0.005	0.008	−0.03	0.01	0.02	−0.018	0.015−	−0.015
24 (RCF + SPSW)	0.015	−0.012	0.03	0.01	−0.006	0.005	0.024	−0.01	0.017	0.001	0.004	0.004	−0.012	−0.004	−0.016	−0.023
4 (RCF)	0.015	0.015	0	0	0.001	0	−0.022	0.007	0.022	0	−0.051	0.43	0.007	−0.007	−0.007	−0.001
8 (RCF)	0.022	0.004	−0.004	0	0	0	−0.018	0	0.022	0	−0.048	−0.037	−0.015	−0.004	0	0
12 (RCF)	0.442	−0.001	0.058	−0.017	0.033	0.033	0.058	−0.05	0.25	0.001	0.375	0	0	−0.017	0	−0.05
24 (RCF)	0.13	0	0.009	0.039	−0.045	0.005	0.009	0.01	0.115	0.002	−0.039	−0.089	−0.064	−0.05	−0.049	−0.042

Table 20: Parameters and effective characteristics in the response of models under group III.

Earthquake parameter	Imperial Valley		Coalinga		Chalfant Valley		Whittier	
	MS	AS	MS	AS	MS	AS	MS	AS
PGA (g)	0.221	0.255	0.519	0.677	0.236	0.447	0.194	0.206
PGAas/PGAms	1.15		1.30		1.89		1.06	
Tg (s)	0.22	0.14	0.12	0.26	0.4	0.2	0.12	0.28
Tg, A/Tg, M	0.64		2.17		0.5		2.33	
tD (s)	12.82	5.74	6.18	0.75	11.5	6.17	7.38	2.85

Table 21: Results of residual drift analysis of models under the MS and SS group III.

Earthquake model	Imperial Valley		Coalinga		Chalfant Valley		Whittier	
	MS (%)	Sequence (%)	MS (%)	Sequence (%)	MS (%)	Sequence (%)	MS (%)	Sequence (%)
4 (RCF + SPSW)	0.004	0.001	−0.01	0.04	0.01	0.02	−0.001	0.008
8 (RCF + SPSW)	−0.001	−0.005	−0.01	−0.01	−0.003	0.01	−0.004	−0.002
12 (RCF + SPSW)	0.005	−0.013	0.002	−0.01	−0.0005	0.007	−0.006	0.007
24 (RCF + SPSW)	0.026	−0.004	0.025	−0.007	−0.047	0.001	−0.003	0.007
4 (RCF)	−0.074	−0.022	0	0	−0.029	0.015	0.015	0
8 (RCF)	−0.015	−0.004	0	0	−0.015	0.004	0.011	0
12 (RCF)	0.054	−0.02	0.022	−0.015	0.037	−0.007	0.039	0.012
24 (RCF)	0.033	−0.004	0.02	−0.023	−0.027	0.022	0.049	0.027

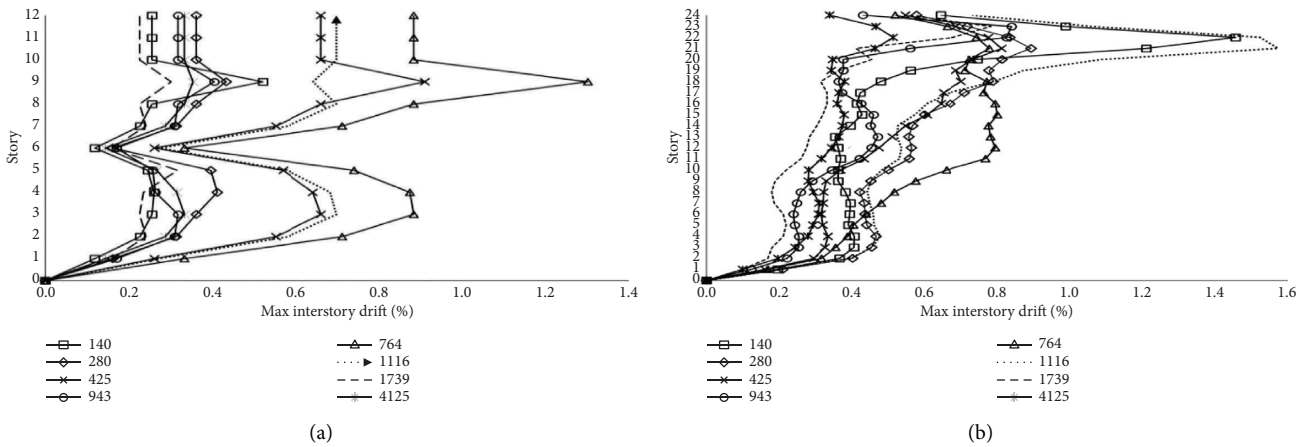

Figure 12: Peak maximum interstory drift of stories under artificial earthquake: (a) 12-story model. (b) 24-story model.

first-mode period of vibration of 0.88 seconds, did not have a resonance displacement response due to its close to the frequency content of any of the MS in this group. The maximum displacement of the stories of the 24-story model has not been increased by the first-mode period of vibration of 1.56 seconds due to not being close to the frequency content of any of the earthquakes of this group. Table 17 presents the effective characteristics of earthquakes in this group.

Table 7 shows the first mode period of vibration and damaged period of the models under group II.

As shown in Table 18, SS has induced to a change in the structural performance. This indicates a significant increase in structural demand in the SS compared to the MS.

As shown in Table 19, it can be considered that AS in some of these groups changed the magnitude and direction of residual drift, and in some other groups, earthquakes remained constant.

4.3. Seismic Demands of Models under MS and SS Group III (Ratio PGA as to MS Greater than 1) [16]. Table 20 shows the first-mode period of vibration and damaged period of the models under group III.

In Table 8, the first-mode period of vibration of models and period of damaged of models under group III were presented.

As shown in Table 19, the residual drift of the models according to some sequences of earthquakes of this group changed direction, some increased, and some other earthquakes did not change.

4.4. Seismic Demands of Models under Artificial SS Group IV. The peak maximum interstory drift of 12- and 24-story models with RCF with SPSW system under the scaled earthquakes of group IV has been displayed in Figure 12.

Table 22: Parameters and effective characteristics in the response of models under artificial SS.

Earthquake	Tabas	Trinidad	Taiwan Smart1	Northridge1	Loma Prieta	Kobe	Northridge6	Parkfield
PGA (g)	0.105	0.147	0.028	0.067	0.285	0.233	0.373	0.103
Tg (s)	0.24	0.16	0.6	0.22	0.46	0.60	0.22	0.22
tD (s)	24.18	11.18	15.25	12.30	8.92	11.59	7.94	11.28

Table 23: The period of damaged of the models under artificial SS.

Tabas model earthquake		Trinidad	Taiwan Smart1	Northridge1	Loma Prieta	Kobe	Northridge6	Parkfield
4 (RCF + SPSW)	0.42	0.34	0.38	0.401	0.36	0.46	0.40	0.36
8 (RCF + SPSW)	0.93	0.72	0.85	0.89	0.74	0.77	0.89	0.81
12 (RCF + SPSW)	1.07	1.07	1.16	1.04	1.16	1.15	1.05	1.04
24 (RCF + SPSW)	1.79	1.80	1.92	1.99	2.11	2.01	1.92	1.86
4 (RCF)	1.21	1.18	1.50	1.20	1.62	1.50	1.31	1.18
8 (RCF)	1.14	1.19	1.38	1.25	1.45	1.16	1.25	0.98
12 (RCF)	2.07	1.74	1.67	2.20	2.38	2.35	2.07	1.63
24 (RCF)	2.29	2.68	3.10	2.84	3.07	3.05	2.97	2.21

Table 24: Different scenarios of sequence earthquakes.

	S1	S2	S3	S4
1	0.3gFF + 015gFF	0.3gNF + 015gFF	0.3gNF + 015gNF	0.3gFF + 015gNF
2	0.3gFF + 0.3gFF	0.3gNF + 0.3gFF	0.3gNF + 0.3gNF	0.3gFF + 0.3gNF
3	0.3gFF + 0.45gFF	0.3gNF + 0.45gFF	0.3gNF + 0.45gNF	0.3gFF + 0.45gNF
4	0.3gFF + 0.60gFF	0.3gNF + 0.60gFF	0.3gNF + 0.60gNF	0.3gFF + 0.60gNF

As shown in Table 19, the predominant AS period was variable from 0.16 to 0.6, and MS and artificial AS have duration time relative much (Table 19).

4.4.1. Results of SS Analysis of Scenarios S1, S3. Scenario S1 includes earthquakes in the far-field of Table 21, and Scenario S3 includes earthquakes in the near-field. This scenario uses a back-to-back or repetitive approach to generate artificial earthquakes using the MS. In this approach, the model is first scaled under the MS, and the dynamic analysis is nonlinear, and then, after free vibration, the AS is applied to the model with different intensities from the MS. It should be noted that the Rayleigh damping coefficients are calculated with the periods of the damaged structure at the end of the MS and are used in the software code. For example, the results of nonlinear dynamic analysis of a 4-story model under a repetitive sequence near-field the Kobe earthquake (Scenario S3) with different scales of 0.5, 0.5, 1.5, 2 AS compared to the MS are presentedin Figure 20. The SS in the repetition method has increased the maximum displacement response of this model more than the maximum displacement response of the MS. The iteration method is more critical than the randomized method in the peak maximum interstory drift and displacement. AS at a scale of 0.5 compared to the MS is increased by about 50%, at a scale of 0.2 by about 62% increased the model response to the response of the MS (Figure 13). Comparing of the ratio of damage period of the 4-story model (Table 21) with the predominant AS period of Table 20 shows that the closest frequency content in Kobe earthquake, the mentioned ratio is 0.76 and the result is resonance the response of AS [40].

4.4.2. Results of SS Analysis of Scenarios S2, S4. Scenario S2 includes the main near-field earthquake and near-field AS (Table 21), and Scenario S4 includes the main near-field earthquake and near-field. For example, the results of nonlinear dynamic analysis of a 4-story model under a randomized SS of the S4 scenario of a Northridge1 far-field earthquake with AS near-field Loma Prieta to different scales of 0.5, 0.1, 1.5, 2 compared to the MS show that the AS in the sequence by the randomized method has increased the maximum displacement response of this model more than the maximum displacement response of the MS and has increased the scale ratio of 2 from 12 cm to 14 cm by about 17%. Comparing of the ratio of damage period of the 4-story model (Table 21) with the predominant AS period of Table 20 shows that the closest frequency content in Kobe earthquake, the mentioned ratio is 0.74 and the result is resonance the response of AS. The maximum of residual drift of the 4-story model under this MS −0.07% and under SS with the mentioned scales −0.18%, −0.38%, −0.49%, and −0.22%, respectively. In estimating the seismic drift demand of the models, the randomized method is critical compared to the iteration method, and in the randomized method of scenario S4, the combination of the MS of the far-field and the AS of the near-field is more critical than the S2 scenario. In SS, high-rise structures with an RCF equipped with SPSW, the demand of residuals drift of the stories, have much better performance than mid-rise structures, and mid-rise structures have better performance than low-rise structures.

According to this study, the performance of structural models in scenario S4 (the MS of the far-field and AS of the near-field earthquake) compared to scenario S2 (the MS of

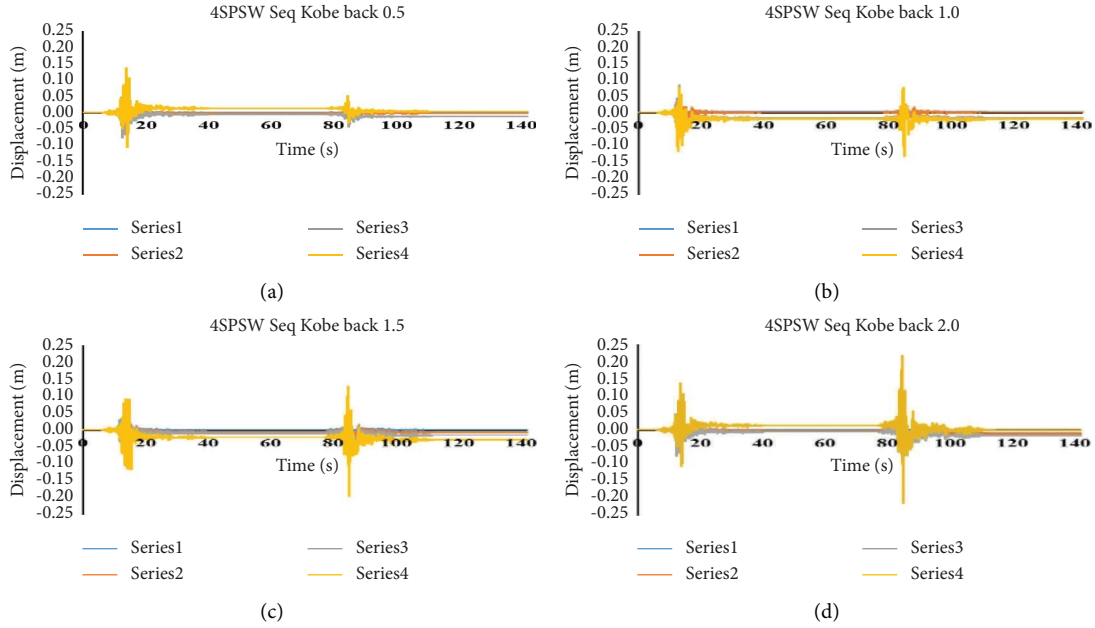

FIGURE 13: Time history of displacement of the 4-story model under Kobe earthquake repetitive sequence. (a) Scale 0.5, (b) scale 1, (c) scale 1.5, (d) scale 2.

the near-field earthquake and AS of the far-field) is more critical. This means that AS near-field causes more damage to the structure and indicates the importance of AS intensity in a SS that AS with a magnitude greater than 1.0 has a major impact on the occurrence of damage and reduced performance of structures compared to a single earthquake.

5. Estimation of Ductility Demands of Models under SS

This section evaluates the peak ductility demands for the SS. As mentioned earlier, SS increases peak displacement and peak ductility demands of structural compared to MS. The peak story displacement parameter is used to calculate the total ductility coefficient μ, as follows:

$$\mu = \frac{u_{\max}}{u_y}, \tag{9}$$

where $u_{\max}$ is the peak displacement of the structure, and u_y is the yield displacement of the structure. To estimate the cumulative ductility of the SS, equation (10) is presented [16].

$$\mu_{\text{seq}} = 1 + \left[\sum_{i=1}^{n} \langle \mu_i - 1 \rangle^p\right]^{1/p}. \tag{10}$$

In equation (10), which is an exceptional function, and given that the cumulative ductility due to SS is always greater than the ductility, each earthquake is considered as an AS the mentioned function is used. Where μ_{seq} is cumulative ductility in a SS, including n number of seismic events, μ_i is ductility related to each seismic event. For μ_i less than one, inside the parentheses of expression 7 is equal to zero. For $p = 2.8$, a comparative diagram of the cumulative ductility is obtained from equation (10), and the cumulative ductility resulting from the analysis is presented in Figure 15. Figures 15 and 16(a) show the comparison of cumulative ductility demand results of RCF with and without SPSW models for combining Group 1 and 2 earthquakes, respectively. Figure 15(b) shows the comparison of cumulative ductility demand results of models for group I, and combined earthquakes show the cumulative plasticity of models for combining group II earthquakes. The value of R^2, which shows the correlation of ductility of equation (10) with the ductility obtained from the analyses, is considered appropriate because it is close to 1 (Figures 14 and 15).

6. Effect of SS on Peak Maximum Demand

6.1. Effect of SS on Peak Maximum Ductility Demand of RCF with and without SPSW (Real SS). In RCF with SPSW, for each of the real seismic scenarios, the peak maximum ductility demand and the ratio of this parameter for the sequence to the MS are calculated. As shown in Figure 16, the effects of SS on the peak ductility demand for the sequence to the peak ductility demand MS of models have behaved differently for different PGA ratios of AS to the MS. The ductility demand of the low-rise model for the PGA ratio is 0.28, and the ductility demands of the mid-rise model for the PGA ratio of 0.74 and the high-rise model for the PGA ratio of 0.97 are equal to 1.66, 1.54, and 1.34, respectively. Larger ratios than 1 mean that structural systems require more ductility against sequence earthquakes. In the most critical, in RCF with SPSW, the peak maximum ductility demand due to SS has increased by 79% compared to the MS.

The effects of SS on the peak ductility demand and the ductility demand of the low-rise, mid-rise, and high-rise model RCF for the PGA ratio 1.23, 1.89, and 1.89 are equal to

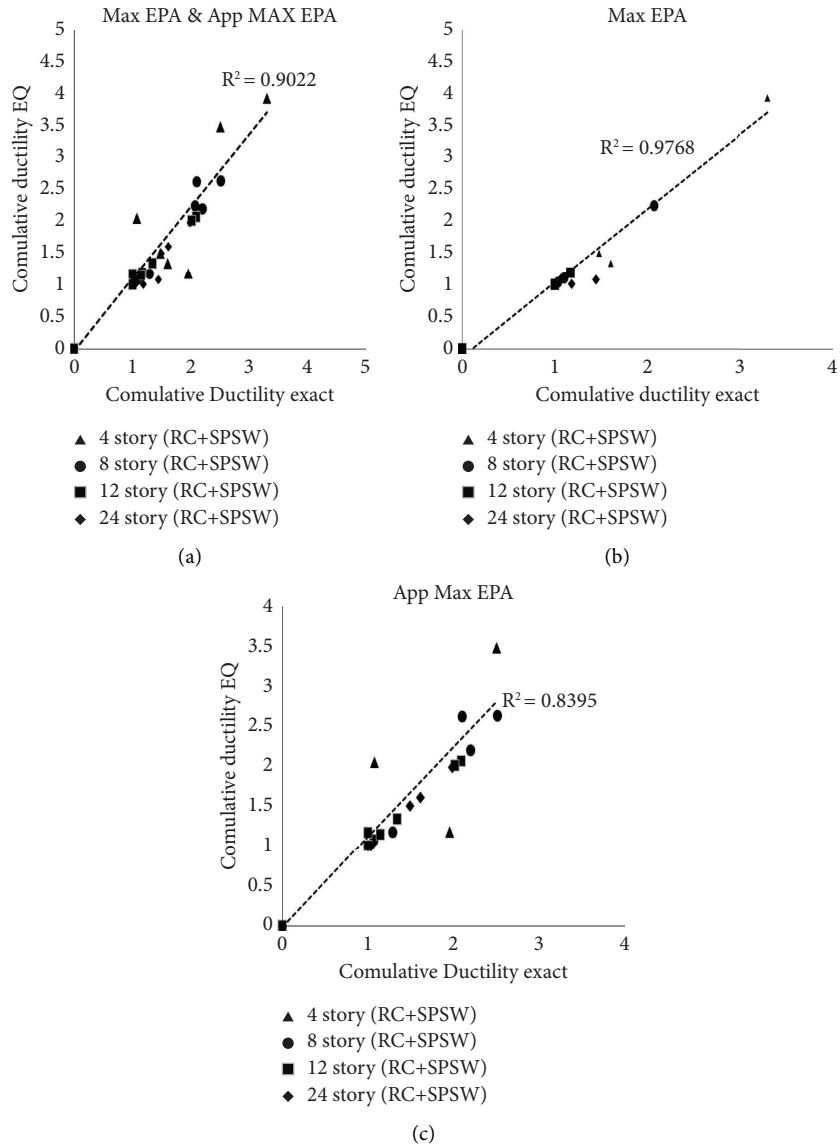

Figure 14: Comparison of cumulative ductility demand of models RCF with SPSW under SS. (a) Group I and II, (b) group I, (c) group II.

Table 25: Results of peak interstory drift demand of models in the MS and SS group III.

Earthquake model	Imperial Valley		Coalinga		Chalfant Valley		Whittier	
	MS (%)	SS (%)	MS (%)	SS (%)	MS (%)	SS (%)	MS (%)	SS (%)
4 (RCF + SPSW)	0.28	0.28	0.24	0.40	0.63	0.45	0.26	0.22
8 (RCF + SPSW)	0.41	0.48	0.3	0.38	0.31	0.48	0.47	0.54
12 (RCF + SPSW)	0.78	0.75	0.45	0.45	0.74	0.74	0.56	0.45
24 (RCF + SPSW)	0.91	0.91	1.46	1.46	1.37	1.37	1.91	1.9
4 (RCF)	1.68	1.68	0.76	1.09	1.04	1.04	1.35	1.35
8 (RCF)	0.99	0.99	0.73	0.95	1.13	1.29	1.01	1.01
12 (RCF)	1.60	1.76	1.65	2.24	2.05	2.05	3.3	3.3
24 (RCF)	2.09	2.42	2.49	2.90	3.77	3.77	5.67	5.67

2.0, 1.89, and 1.42, respectively (Figure 18). Larger ratios than 1 mean that structural systems require more ductility against sequence earthquakes. In the most critical, in RCF, the peak maximum ductility demand due to SS has increased by 100% compared to the MS. Based on the expected use and performance, the structures have ductility criteria corresponding to the MS. Thus, there is a need to review the ductility criteria of structures.

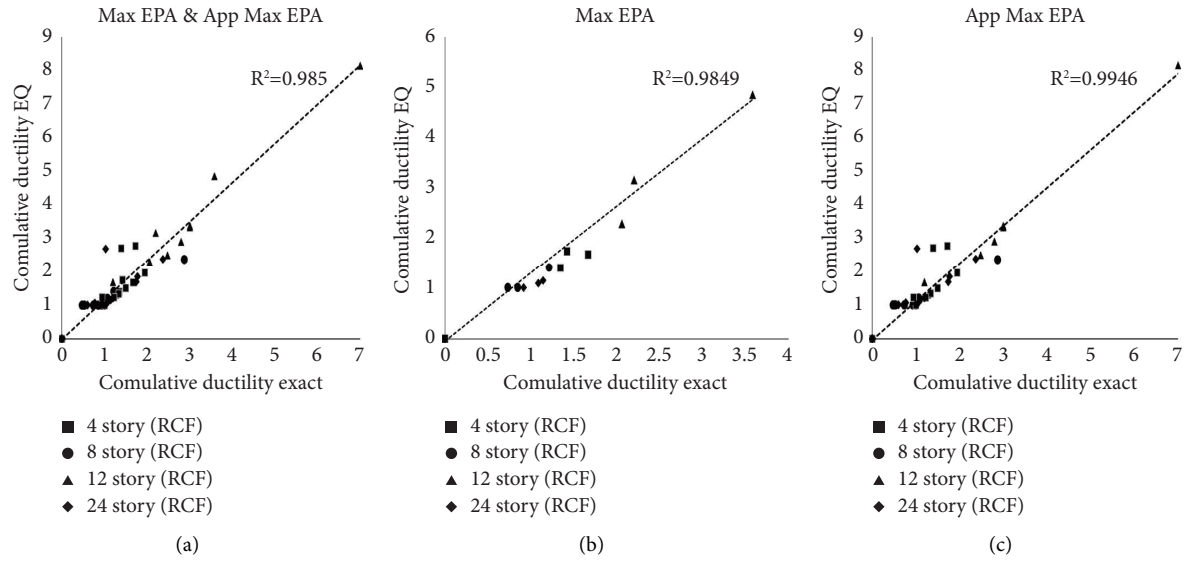

Figure 15: Comparison of cumulative ductility demand of models RCF without SPSW under SS. (a) Group I and II, (b) group I, (c) group II.

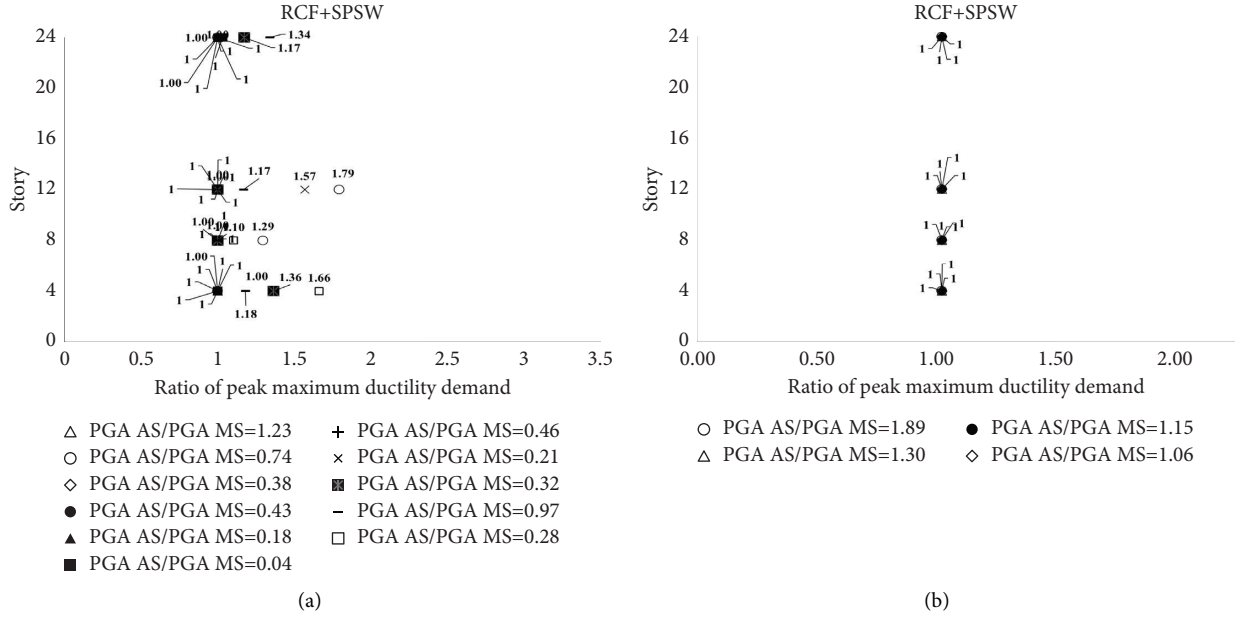

Figure 16: Ratio of peak maximum ductility demand of RCF with SPSW in SS to MS: (a) combination of group I and II, (b) group III.

6.2. Effect of SS on Peak Maximum Inter-Story Drift Demand of RCF with and without SPSW (Real SS). In the 4-story RCF with SPSW model, the peak maximum inter-story drift demand of stories increased 1.9 times compared to the MS in the ratio of AS PGA to the PGA MS of 0.28; in the 8-story model, this increase is 2.31 times compared to the MS in the PGA ratio of 1.89; in the 12-story model, an increase of 1.96 times in the PGA ratio of 1.89; and in the 24-story model, an increase of 2.17 times in the acceleration ratio of 0.43 (Figure 16). This shows that for different models of a RCF with SPSW, the AS PGA ratios to the MS related to the peak interstory drift demand of stories are approximately 0.25 for low-rise models, 2 for mid-rise models, and 0.5 for high-rise models. The maximum increase of the peak inter-story drift demand has been occured in the repetitive method of the artificial seismic scenario. In the 4-story model in the ratio of PGA AS to PGA MS, respectively, 1, 1.5, and 2, this demand is equal, respectively, 1.96, 1.4, and 1 times the demands in the MS, in the 8-story model, this demand is equal to 1.18, 1.98, and 3.40 times the demands in the MS, in the 12-story model, respectively, this demand is equal to 1, 2, and 3.4 times the demand in the MS, and in the 24-story model, this demand is equal to 1, 2, and 3.4 times the demands, respectively, in the MS (Figure 18). In the 4-story with RCF model, the peak maximum inter-story drift demand of stories, 1.70 times is increased compared to the MS in the

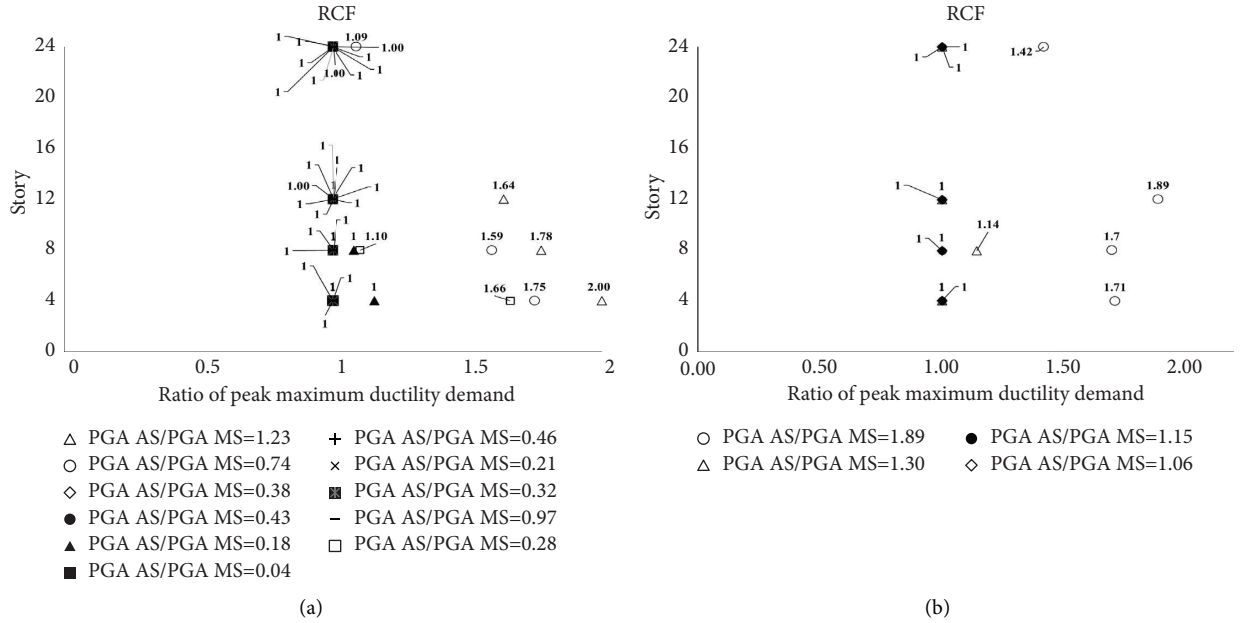

Figure 17: Ratio of peak maximum ductility demand of RCF in SS to MS: (a) combination of group I and II, (b) group III.

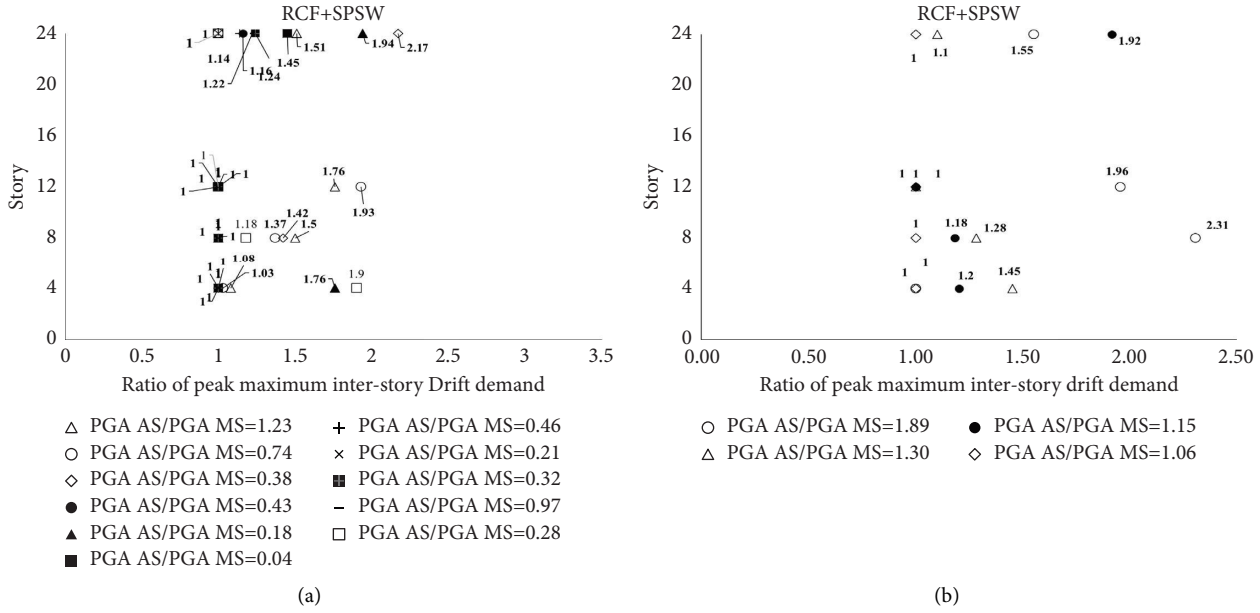

Figure 18: Ratio of the peak maximum interstory drift demand of the real SS of the models to the MS demands under in RCF with SPSW: (a) groups I and II, (b) group III.

ratio of AS PGA to the PGA MS 1.89, in the 8-story with RCF model, this increase is 2.45 times to the MS in the PGA ratio of 1.89, in the 12-story with RCF model, an increase of 2.0 times in the PGA ratio of 1.89 and in the 24-story with RCF model, an increase of 2.02 times in the acceleration ratio of 1.30 (Figure 15). This shows that for different models of a RCF with SPSW, the AS PGA ratios to the MS related to the peak interstory drift demand of stories are approximately 2.0 for low-rise models, 2.0 for mid-rise models, and 1.5 for high-rise models. The maximum increase of the peak inter-story drift demand has been occured in the repetitive method of the artificial seismic scenario. In the 4-story with RCF model in the ratio of PGA AS to PGA MS, respectively, 1, 1.5, and 2, this demand is equal, respectively, 1.65, 2.80, and 4.50 times the demands in the MS, in the 8-story with RCF model, this demand is equal to 1.91, 2.82, and 3.65 times the demands in the MS, in the 12-story with RCF model, respectively, this demand is equal to 1.13, 2, and 5 times the demand in the MS, and in the 24-story model, this demand is equal to 2, 3, and 6 times the demands, respectively, in the

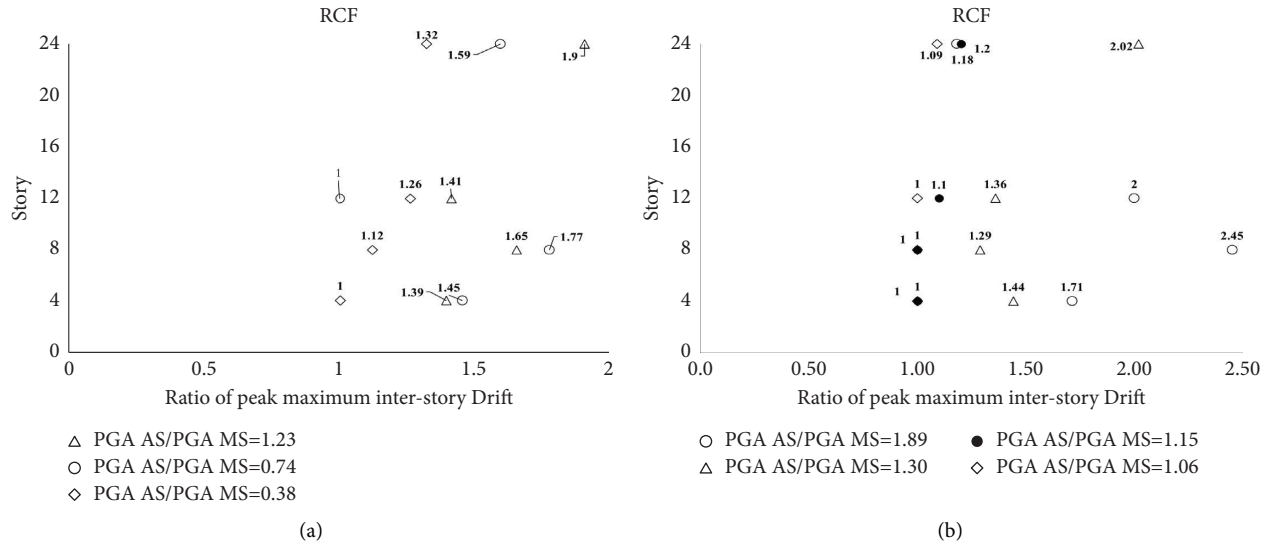

Figure 19: Ratio of the peak maximum interstory drift demand of the real SS of the models to the MS demands under in RCF with SPSW: (a) groups I and II, (b) group III.

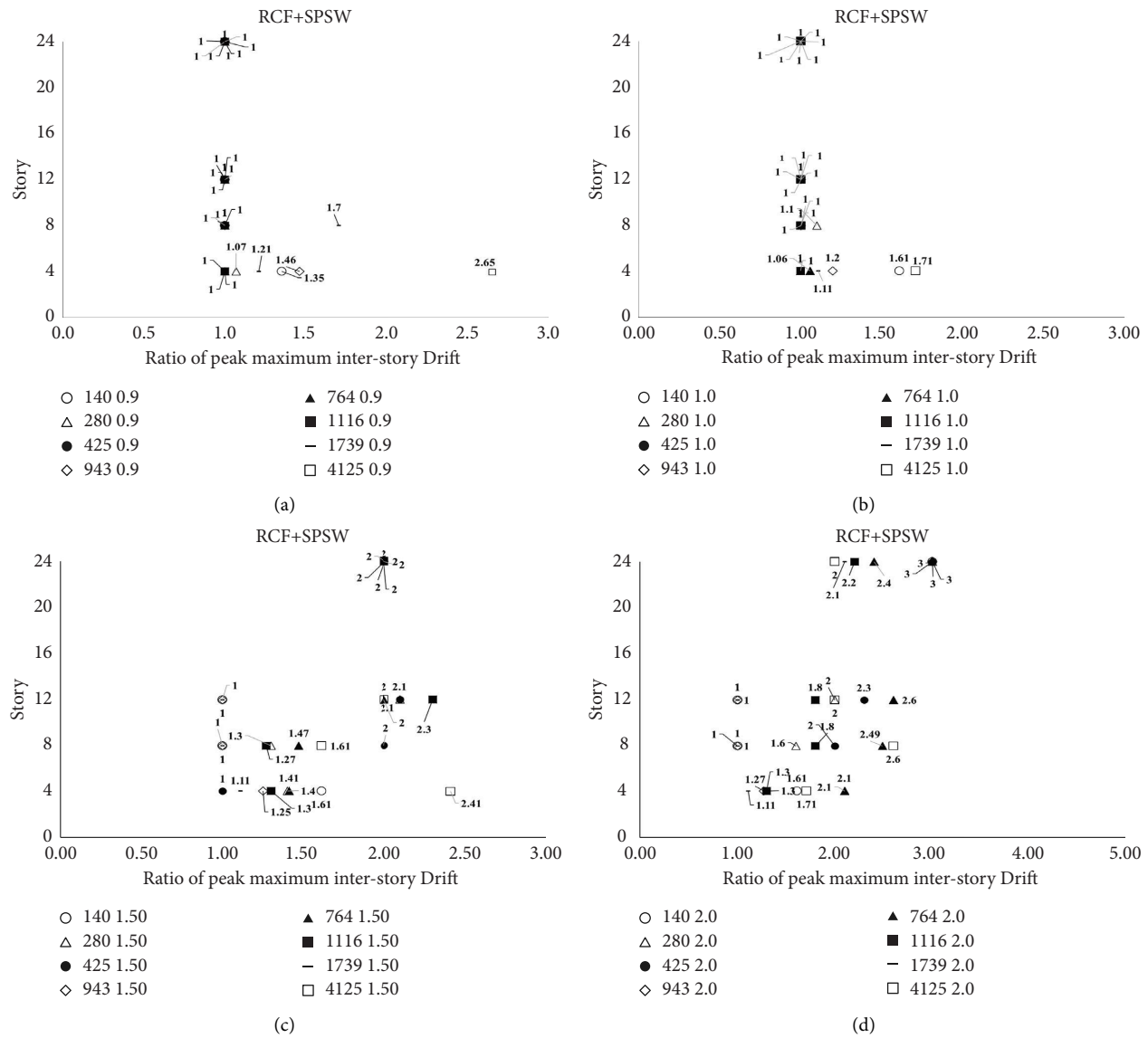

Figure 20: Ratio of peak maximum of interstory drift demand for artificial seismic of models to MS demands of S1 and S3 scenarios in RCF with SPSW: (a) Scale 0.9, (b) scale 1, (c) scale 1.5, (d) scale 2.

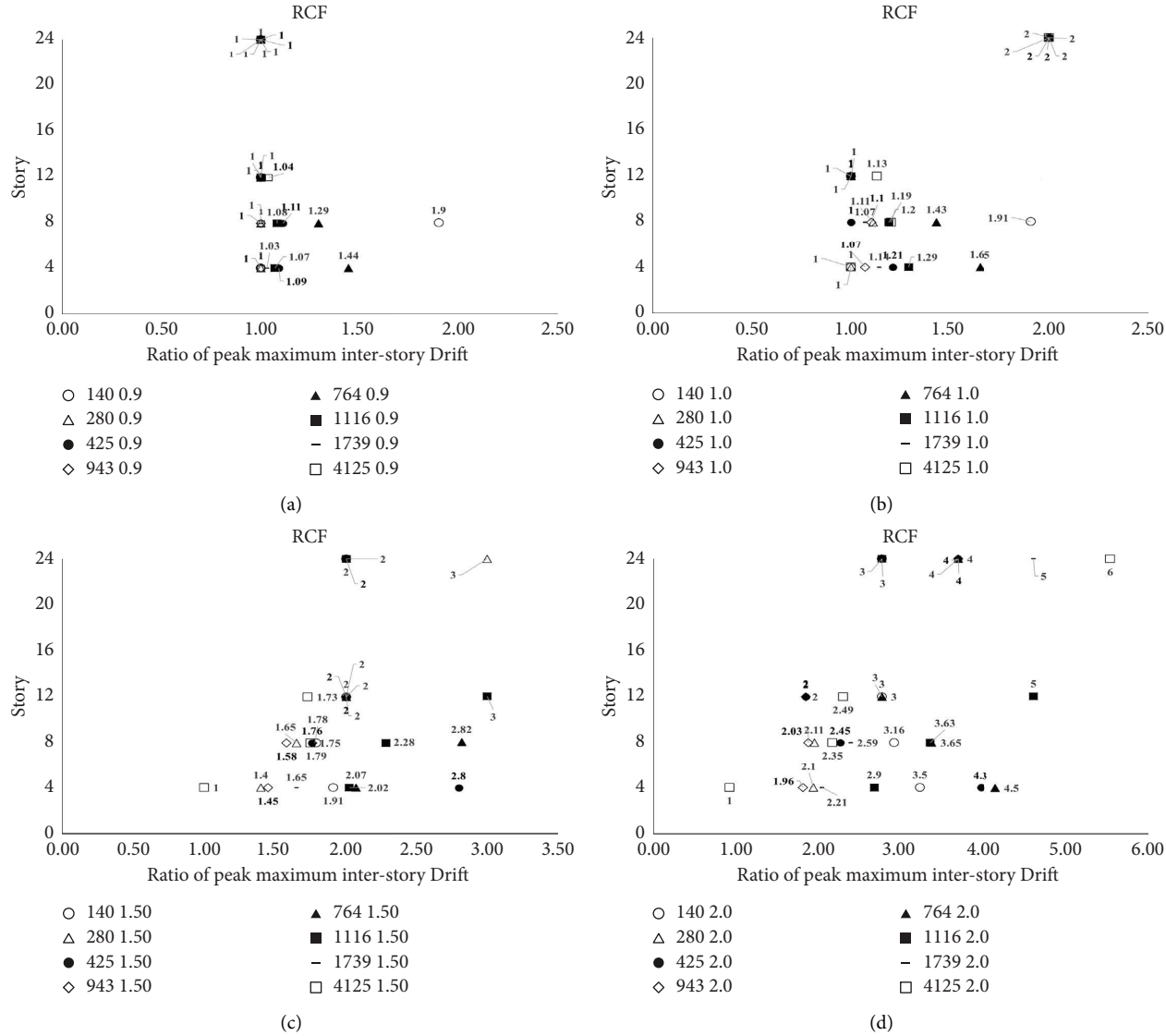

Figure 21: Ratio of the peak maximum interstory drift demand of the real SS of the models to the MS demands under in RCF without SPSW: (a) Scale 0.9, (b) scale 1, (c) scale 1.5, (d) scale 2.

MS (Figure 16). Comparison of the peak ductility demand of RCF equipped with SPSW with the peak ductility demand of RCF equipped with concrete shear walls [45] shows that the peak maximum ductility demand in the critical case due to SS of the 12-story model in this study equivalent to 79% in the ratio of PGA of AS to the PGA of MS is 0.74 (Figure 20), which is increased compared to the MS, and in RCF with concrete shear walls, the peak maximum ductility demand in the critical case due to SS has increased by 72% compared to the case of the MS [45]. In a real SS, the peak ductility demand of RCF with concrete shear walls decreases with increasing the height of the structure, while in RCF with SPSW, the peak ductility demand decreases from 4 story to 8 story. It has increased from 8 story to 12 story and decreased from 12 story to 24 story (Figure21).

6.3. Effect of SS on Peak Maximum Interstory Drift Demand of RCF with and without SPSW (Artificial SS). In the artificial SS, this demand has increased up to a maximum of 3 times to the MS for PGA AS ratio of 2 times when RC is compared with SPSW (Figure 13). While in the artificial SS, this demand has increased up to a maximum of 6 times to the MS for PGA AS ratio of 2 times when RC is compared without SPSW (Figure 20).

7. Conclusion

The use of SPSW as an effective lateral system in seismic rehabilitation to increase the lateral strength and stiffness of RCF against earthquake is considered. In this research, to the assessment of the seismic demands of RCF equipped with SPSW, four models with 4, 8, 12, and 24 story under the real and artificial sequence of four groups of earthquakes with different after-shocks and the finite element software have been used. The resonance phenomenon was observed as a result of the adaptation of the

first-mode period of vibration of the 4-story model and the predominant period of some real earthquakes. According to the analysis, the main results of the research are as follows:

(1) The real seismic sequence increases the ratio of peak of interstory drift of stories by an average of 2 times the similar demand in the main-shock in RCF with and without SPSW. The artificial seismic sequence in PGA after-shock to main-shock equals 2 up to 3.0 times the main-shock in RCF with SPSW, and the artificial seismic sequence in PGA after-shock to main-shock equals 2 up to 6.0 times the main-shock in RCF without SPSW.

(2) In a real seismic sequence, the ratio of critical PGA after-shock to the main-shock related to the peak interstory drift in the RCF with SPSW is not constant, and this ratio is approximately 0.25 for low-rise structures, 2.0 for mid-rise structures, and 0.5 for high-rise structures. In the RCF without SPSW, this ratio is approximately 2.0 for low-rise structures, 2.0 for mid-rise structures, and 1.5 for high-rise structures.

(3) In RCF with and without SPSW, real seismic sequence increases the ratio of maximum ductility demand by 1.52 and 1.65 times in the structure, respectively.

(4) Seismic sequencing can increase the peak maximum interstory drifts demand and the peak maximum ductility demand of models relative to a single earthquake; note that, because the amount of damage to the structure is directly related to the ductility demand, the models after the after-shock experience may cause significant damage.

(5) After-shocks may change the direction and magnitude of residual displacement in real and artificial seismic sequences. Also, in estimating the residual drift of the models, the randomized method of the artificial sequence is more critical than the repetitive method.

(6) According to this research, in determining the peak maximum interstory drift demand and the peak maximum ductility demand of RCF with and without SPSW, the repetitive method in the artificial sequence is more critical than the randomized method. However, in the artificial sequence randomized method, near-field after-shocks caused more damage to the RCF with SPSW than far-field after-shocks.

(7) According to the results of the analysis, it seems that the effect of the seismic sequence should be considered in seismic calculations and seismic design codes due to the increase in the maximum ductility demands and the maximum interstory drift demands of a RCF with and without SPSW compared to the main-shock.

Data Availability

The data used to support the findings of this study are available from the corresponding author upon request.

Conflicts of Interest

The authors declare that they have no conflicts of interest.

References

[1] Y. Dong and D. M. Frangopol, "Risk and resilience assessment of bridges under main-shock and after-shocks incorporating uncertainties," *Engineering Structures*, vol. 83, pp. 198–208, 2015.

[2] H. Gavin and W. David, *The 03/11/2011 Mw9.0 Tohoku, Japan Earthquake*, U.S. Geological Survey, National Earthquake Information Center, 2011.

[3] C. H. Zhai, E. P. Wen, S. Li, and L. L. Xie, "The influences of seismic sequence on the inelastic SDOF System," *Proc, 15th world World Conf. on earthquake engineering*, vol. 4, pp. 2947–2954, 2012.

[4] M. Hatzivassiliou and G. D. Hatzigeorgiou, "Seismic sequence effects on three-dimensional reinforced concrete buildings," *Soil Dynamics and Earthquake Engineering*, vol. 72, pp. 77–88, 2015.

[5] F. Omori, "On the after-shocks of earthquakes," *Journal of the College of Science*, vol. 7, no. 2, pp. 111–200, 1894.

[6] S. A. Mahin, "Effects of duration and after-shocks on inelastic design earthquakes," *The seventh world conference on earthquake engineering*, vol. 5, pp. 677–680, 1980.

[7] A. S. Elnashai, J. J. Bommer, and A. Martinez-Pereira, "Engineering implications of strong-motion records from recent earthquakes," in *Proceedings of the eleventh European Conference on Earthquake Engineering*.

[8] Sunasaka, "Strength demand spectra with uniform damage level in lifetime of structure," *Journal of Structural Engineering*, vol. 48A, no. 6, pp. 523–530, 2002.

[9] C. Amadio, M. Fragiacomo, and S. Rajgelj, "The effects of repeated earthquake ground motions on the non-linear response of SDOF systems," *Earthquake Engineering & Structural Dynamics*, vol. 32, no. 2, pp. 291–308, 2003.

[10] S. Das, V. K. Gupta, and V. Srimahavishnu, "Damage-based design with no repairs for multiple events and its sensitivity to seismicity model," *Earthquake Engineering & Structural Dynamics*, vol. 36, no. 3, pp. 307–325, 2007.

[11] M. Iancovivi and I. Georgiana, "Evaluation of the inelastic demand of structures subjected to multiple ground motions," *Structural Engineering*, vol. 42, pp. 143–154, 2007.

[12] G. D. Hatzigeorgiou and D. E. Beskos, "Inelastic displacement ratios for SDOF structures subjected to repeated earthquakes," *Engineering Structures*, vol. 31, no. 11, pp. 2744–2755, 2009.

[13] G. D. Hatzigeorgiou, "Behavior factors for nonlinear structures subjected to multiple near-fault earthquakes," *Computers & Structures*, vol. 88, no. 5-6, pp. 309–321, 2010.

[14] G. D. Hatzigeorgiou, "Ductility demand spectra for multiple near and far-fault earthquakes," *Soil Dynamics and Earthquake Engineering*, vol. 30, no. 4, pp. 170–183, 2010.

[15] A. Moustafa and I. Takewaki, "Response of nonlinear single-degree-of-freedom structures to random acceleration

sequences," *Engineering Structures*, vol. 33, no. 4, pp. 1251–1258, 2011.

[16] G. D. Hatzigeorgiou and A. A. Liolios, "Nonlinear behaviour of RC frames under repeated strong ground motions," *Soil Dynamics and Earthquake Engineering*, vol. 30, no. 10, pp. 1010–1025, 2010.

[17] J. Ruiz-García and J. C. Negrete-Manriquez, "Evaluation of drift demands in existing steel frames under as-recorded far-field and near-fault main-shock-after-shock seismic sequences," *Engineering Structures*, vol. 33, no. 2, pp. 621–634, 2011.

[18] S. Efraimiadou, G. D. Hatzigeorgiou, and D. E. Beskos, "Structural Pounding between Adjacent Buildings Subjected to strong Ground Motions," *Part I: The effect of different structures arrangement. Earthquake Engineering & Structural Dynamics*, vol. 42, 2013.

[19] L. Di Sarno, "Effects of multiple earthquakes on inelastic structural response," *Engineering Structures*, vol. 56, pp. 673–681, 2013.

[20] A. E. Abdelnaby and A. S. Elnashai, "Performance of degrading reinforced concrete frame systems under the Tohoku and christchurch earthquake sequences," *Journal of Earthquake Engineering*, vol. 18, no. 7, pp. 1009–1036, 2014.

[21] J. Shin, J. Kim, and K. Lee, "Seismic assessment of damaged piloti-type RC building subjected to successive earthquakes," *Earthquake Engineering & Structural Dynamics*, vol. 43, no. 11, pp. 1603–1619, 2014.

[22] S. R. Salimbahrami and M. Gholhaki, "Analytical study to evaluate the effect of higher modes of reinforced concrete moment-resisting frames with thin steel shear wall under simple pulse," *Advances in Structural Engineering*, vol. 21, no. 15, pp. 2311–2325, 2018.

[23] L. Di Sarno and F. Pugliese, "Seismic fragility of existing RC buildings with corroded bars under earthquake sequences," *Soil Dynamics and Earthquake Engineering*, vol. 134, pp. 106169–106178, 2020.

[24] L. Di Sarno and J. R. Wu, "Fragility assessment of existing low-rise steel moment-resisting frames with masonry infills under main-shock-after-shock earthquake sequences," *Bulletin of Earthquake Engineering*, vol. 19, no. 6, pp. 2483–2504, 2021.

[25] L. Di Sarno and F. Pugliese, "Effects of mainshock-aftershock sequences on fragility analysis of RC buildings with ageing," *Engineering Structures*, vol. 232, Article ID 111837, 2021.

[26] A. Astaneh-Asl, *Seismic Behavior and Design of Steel Shear Walls*, Steel Technical Information and Product Services Report, Structural Steel Educational Council, Moraga, CA, 2001.

[27] T. Görgülü, Y. S. Tama, S. Yilmaz, H. Kaplan, and Z. Ay, "Strengthening of reinforced concrete structures with external steel shear walls," *Journal of Constructional Steel Research*, vol. 70, no. 1, pp. 226–235, 2012.

[28] I. R. Choi and H. G. Park, "Cyclic loading test for reinforced concrete frame with thin steel infill plate," *Journal of Structural Engineering*, vol. 137, no. 6, pp. 654–664, 2011.

[29] S. Mazzoni, S. McKenna, F. Scott, and G. L. Fenves, "OpenSees command language manual," *Pacific Earthquake Engineering Research (PEER) Center*, vol. 264, 2006.

[30] S. Sabouri, *Introduction to SPSW*, Nashr Anghize Publications, Tehran, Iran, 2013.

[31] B. Stafford Smith, *Coull A High-Rise Building Structures: Analysis and Design*, Tehran, Iran, 1991.

[32] Iranian National Building Code, *Applied Loads on Buildings. Part 6*, Ministry of Roads & Urban Development, Tehran, Iran.

[33] Iranian National Building Code, *Design and Implement of Concrete Buildings. Part 9*, Ministry of Roads & Urban Development, Tehran, Iran, 2013.

[34] I. S. Code, *Iranian Code of Practice for Seismic Resistant Design of Buildings 2800*, Ministry of Roads & Urban Development, Tehran, Iran, 4th ed edition, 2014.

[35] American Society of Civil Engineers (Asce), *Minimum Design Loads for Buildings and Other Structures*, ASCE07, 2010.

[36] J. Ruiz-García, "Main-shock-After-shock ground motion features and their influence in buildings seismic response," *Journal of Earthquake Engineering*, vol. 16, no. 5, pp. 719–737, 2012.

[37] A. Faisal, T. A. Majid, and G. D. Hatzigeorgiou, "Investigation of story ductility demands of inelastic concrete frames subjected to repeated earthquakes," *Soil Dynamics and Earthquake Engineering*, vol. 44, pp. 42–53, 2013.

[38] G. G. Amiri and F. M. Dana, "Introduction of the most suitable parameter for selection of critical earthquake," *Computers & Structures*, vol. 83, no. 8-9, pp. 613–626, 2005.

[39] D. Vamvatsikos and C. A. Cornell, "Incremental dynamic analysis," *Earthquake Engineering & Structural Dynamics*, vol. 31, no. 3, pp. 491–514, 2002.

[40] V. Seismosignal, "A computer program for signal processing of timeistories, University of Berkley California, USA.

[41] E. Miranda, "Evaluation of site-dependent inelastic seismic design spectra," *Journal of Structural Engineering*, vol. 119, no. 5, pp. 1319–1338, 1993.

[42] J. Ruiz-García, M. V. Marin, and A. Terán-Gilmore, "Effect of seismic sequences in reinforced concrete frame buildings located in soft-soil sites," *Soil Dynamics and Earthquake Engineering*, vol. 63, pp. 56–68, 2014.

[43] C. H. Zhai, W. P. Wen, S. Li, Z. Chen, Z. Chang, and L. L. Xie, "The damage investigation of inelastic SDOF structure under the main-shock–after-shock sequence-type ground motions," *Soil Dynamics and Earthquake Engineering*, vol. 59, pp. 30–41, 2014.

[44] C. H. Zhai, W. P. Wen, Z. Chen, S. Li, and L. L. Xie, "Damage spectra for the main-shock–after-shock sequence-type ground motions," *Soil Dynamics and Earthquake Engineering*, vol. 45, pp. 1–12, 2013.

[45] G. Ghodrati Amiri, H. Rajaei Lak, and E. Rajabi, "Effects of seismic sequence on increased response of concrete moment frames with and without shear wall," *Amirkabir Journal of Civil Engineering*, vol. 50, pp. 845–854, 2018.